International Journal of
Young Scientist Research

Vol 6, No1, Dec 2022
ISSN: 2588- 5111

Contents

Young Scientist Research

Title proper: Young Scientist Research

Subject: NATURAL SCIENCES, ART, ENGINEERING AND TECHNOLOGY

Corporate contributor: Ariaian Young Innovative Minds Institute

Publisher: Tehran: Ariaian Young Innovative Minds Institute

Dates of publication: 2017- Present

Frequency: Annual

Type of resource: Periodical

Language: English

Country: Iran

Medium: Online

Indexed by: ROAD (The Directory of Open Access Resources)

ISSN- 2588-5111
ISSN International Centre
45 rue de Turbigo
75003 Paris
France

Address:

Unit 14, No.32, Malek Ave., Shariati St.

Post Code: 1565843537

Tel:+9821-77507013, 77522395

WELCOME TO THE INTERNATIONAL JOURNAL of YOUNG SCIENTIST RESEARCH

Young Scientist Research is a research journal based on scientific projects and we are pleased to present our students' work in scientific activities. This open-access journal includes young students' research in any field of science which publishes full-length and abstract research on any aspects of applied sciences in relation to work presented in both national and international conferences, competitions and tournaments of all types.

Programs that have educational opportunities for high school students to present their distinguished projects from regional, national and international events such as International Conference of Young Scientists (ICYS), International / Persian Young Physicists' Tournament (IYPT/ PYPT), International / Iran Physics' Tournament (IPT/ IRPT), International Music , Science , Engineering Fair (IMSEF).

New manuscripts sent to the Journal will be handled by the Editorial Office who checks compliance with the guidelines to authors. Then a rapid screening process at which stage a decision to reject or to go to full review is made.

By submission of a manuscript to the Journal, all authors warrant that they have the authority to publish the material and that the paper, or one substantially the same, has neither been published previously, nor is being considered for publication elsewhere.

This journal belongs to Ariaian Young Innovative Minds Institute, AYIMI, and one to two issues are published in a year. All details are on the YOUNG SCIENTIST RESEARCH Journal website (http://journal.ayimi.org)

Editor in Chief
Dr. Dina Izadi
Researcher & President of
AYIMI , International Research Institute
ADIB, Cultural and Artistic Institute
http://www.ayimi.org
http://www.ayimi.org/adib
http://journal.ayimi.org
Email: info@ayimi.org
Unit 14, No. 32, Malek Ave., Shariati St.,
Post Code: 1565843537
Tehran/ Iran

CURRENT ISSUE
Vol 6 NO 1 DEC 2022

THE PROBABILITY OF A CYLINDRICAL DICE TO BE LUCKY

Yas Meshkin, Farzanegan 2 high school, Tehran, Iran, meshkinyas@gmail.com

ARTICLE INFO

Participated in PYPT, IYPT 2022

Advisors: Alireza Noroozshad, Mohammad Shariatmadar

Accepted in country selection by Ariaian Young

Innovative Minds Institute , AYIMI

http://www.ayimi.org ,info@ayimi.org

ABSTRACT

A coin is a circular disk so when its flipped it lands on either its heads or tails but technically it's really thin cylinder so there's a tiny chance for it to land on its edge. Dice are generally used to generate a random outcome in which the physical design and quantity of the dice thrown determines the mathematical outcome used mostly for different games all around the world but in this research we are going to find the most important factors in a cylindrical dice when we flip it to land on each one of the faces.

Keywords : *Cylindrical Dice, Probability, Mass Theory*

1. Introduction

The problem states that to land a coin on its side is often associated with the idea of a rare occurrence. What should be the physical and geometrical characteristics of a cylindrical dice so that it has the same probability to land on its side and one of its faces? (Fig.1).

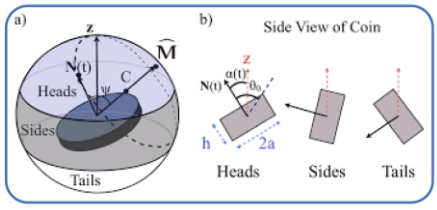

Fig.1: Paper spiral suspended above a candle

A coin is a circular disk so when its flipped it lands on either its heads or tails but technically it's really thin cylinder so there's a tiny chance for it to land on its edge but that's such a small probability that it doesn't even matter but there's also something like a pen which is the other extreme a very long cylinder if we flip it, it would land on its edge and if the pen was to be a coin the chance of the landing on its faces would be so little. So somewhere between the coin and the pen there's a cylindrical thick enough which makes it as likely to land on its edge and one of its faces and can be used as a three sided dice.

Dice is generally used to generate a random outcome in which the physical design and quantity of the dice thrown determines the mathematical outcome used mostly for different games all around the world. A cylinder on the other hand doesn't have an abundance of symmetry for various reasons least of it being the edge face doesn't have the same shape as the other two faces.

2. Theories and Methods

we inscribe the circular in a sphere. A cylindrical dice is made of two pieces; the smaller part is denser than the bigger one and they have equal masses, this moves the center of mass from the middle closer to the edge of the cylinder. The important way and variables such as height and angular velocity directly affect the throw's outcome. The number of throws is 1500 which the probability of getting an edge, P, is a third and 1-P is the probability of not getting an edge (2/3). Using these values, we can get a probability based on a normal approximation.

2.1. Center of Mass Theory

In this theory , considering that the center of mass is right in the middle of the cylinder , we divide the cylinder into 3 parts from the inside , each of which represents one of the faces . This theory states that all 3 parts should have the same mass (Fig. 2).

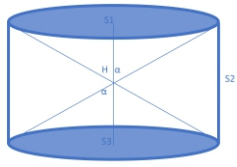

Fig.2: The cylinder is divided into 3 parts from the inside

2.2. Sphere theory

In throwing a sphere shaped ball the probability of it landing on any point on it is equal and this is where the idea comes from. This thick coin is embedded in a sphere where it fits the idea is that if we throw the sphere which has the thick coin inside of it one third of the area of the surface of the sphere is associated with one face one third a it is associated with the other face and the third associated with the band around the middle which is the edge (Fig.3) (Eqs. 1-4).

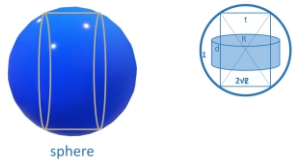

Fig.3: Thick coin is embedded in a sphere

$$S = 2\pi t R \quad (1)$$

$$S = \frac{4\pi R^2}{3}$$

$$t = \frac{2R}{3} \Rightarrow 2R = 3t \quad (2)$$

$$D^2 + t^2 = (2R)^2 = (3t)^2 \quad (3)$$

$$D^2 + t^2 = 9t^2 \quad (4)$$

$$D^2 = 8t^2 \qquad D = 2\sqrt{2}t$$

2.3. 2D Version

Now let's look at it from a 2d perspective. The coin is now fitted in a circle so taking the rectangular cross section of the disk and doing essentially the same technique but it 2d which means dividing the perimeter of the circle into third which means dividing the perimeter of the circle into thirds (Eqs. 5-7) (Fig. 4).

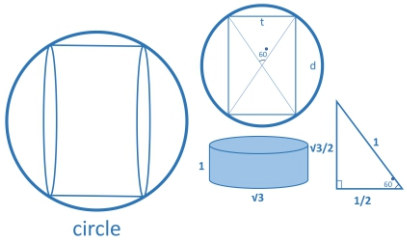

Fig. 4: The coin is now fitted in a circle

$$D = 2R \sin 60^0 = R\sqrt{3} \quad (5)$$

$$t = 2R \cos 60^0 = R \quad (6)$$

$$\boldsymbol{D = \sqrt{3}t} \quad (7)$$

So with the first 2 theories we found the shortest and the tallest extremes then with the third theory we got ratio diameter to thickness but they are both super theoretical and non-might be right so the only way to prove that they are right is an experiment repeated hundreds of times keeping all the factors except the ratio diameter to thickness constant in order to find the ideal ratio that gives the third probability .

3. Experiment

First I did 3D Printed Cylinders with ratio diameter thickness of route two and route 3 with the same mass and material.

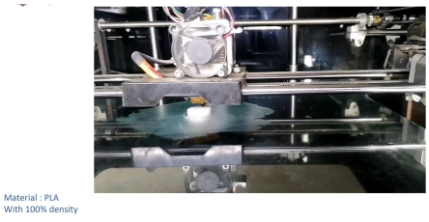

Fig. 5: 3D Printed Cylinders

Random Throw :then I figured out a way to a random throw . It's important the way the cylinders are thrown cause it has a direct effect on the outcome . The throw has to be random but not every single parameter has to be random in the throw . Variables like height and angular velocity directly affect on the throw's outcome . The angle which the cylinders are thrown at , is the random parameter in this method .

4. Statistical Analysis

Here we assume that the probability of a third landing on each side is correct with the given ratios and then calculate the likeliness of our data if that's true (specifically the edge). What is the chance of seeing 395 edges if it's got probability of third ?

we can calculate that using binomial distribution which says from our 1500 throws we got 395 edges if the probability of success (an edge) is a third what is the chance of that happening ? The answer is a very tiny probability but this isn't surprising considering that this is the probability of exactly 395 edges so what we do instead is saying what is the probability of getting less than or equal to 395 edges ; we'd need to calculate the probability of 1 + the probability of 2 + all the way to the probability of 395 which with the binomial distribution that would take lots of time and is unnecessary so instead we approximate it using the normal distribution . Our expectation is 500 if we're right (that's from our binomial distribution) . We also get our variance from binomial distribution (the number is 1500 that's how many throws , P is a third (probability of getting an edge) and 1-P is the probability of not getting an edge (2/3) (Fig. 6). We can use these numbers to see how wide this bell curve needs to be . Using these values we can get a probability based on a normal approximation .

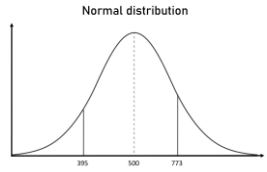

Fig. 6: Variance from binomial distribution

We got our average value here (this is what we would expect if it was a third) and we are saying what is the probability of 395 and how far away is it ? And it's still really tiny ; and even if we took a 2 sided test to see if it's in the extreme it would still be tiny . So we wouldn't have gotten these numbers if the ratios were correct . The probability of getting an edge is statistically different from a third with the 2 ratios. Although both the ratios were incorrect , they provided upper and lower bounds on the answer ; so I made cylinders with ratio diameter to thicknesses between $2\sqrt{2}$ and $\sqrt{3}$ (started with the $2\sqrt{2}$ ratio and made each cylinder 1 millimeter thicker to $\sqrt{3}$) (Fig.7a & b).

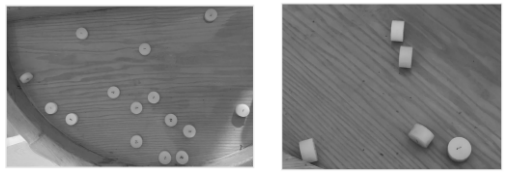

(a) (b)

Fig. 7: a)Thinnest cylinder $2\sqrt{2}$ b) Thickest cylinder

From the chart the closest ratio to the third probability is 2.4. As shown the probability is a big number , and the difference from the third probability is less than 2% (Tables 1 &2).

Table 1: Ratio $2\sqrt{2}$for total number of throws 1500

Number of	The results number	The expected number	The difference	Percentage
landing on one of its faces	1105	1000	105	73.66%
landing on its edge	395	500	-105	26.33%
landing on face 1	553	500	53	36.86%
landing on face 2	552	500	52	36.81%

Table 2: Ratio $\sqrt{3}$ for total number of throws 1500

Number of	The results number	The expected number	The difference	percentage
landing on one of its faces	727	1000	-273	48.47%
landing on its edge	773	500	273	51.53%
landing on face 1	351	500	-149	23.41%
landing on face 2	376	500	-124	25.06%

With an experiment like this it's about having the result close enough and 2.4 can be considered close enough but we can get even closer than that .

I made a cylindrical dice of two pieces ; the smaller part is denser than the bigger one and they have equal masses , this moves the center of mass from the middle closer to the edge of the cylinder .This cylindrical dice is landed and the percentage of landing on the edge ,the heavier side, is more and this is where the idea of the mass theory comes from .

Then we experimented with 3D printed dice and the mass theories cylinders with ratio diameter to thicknesses of 2√2 , √3 and 2.4 with following results (Eqs. 8-13).

n=1500 P=1.3

Probability of Edge for 2√2 :

$$P(X=395)=\binom{1500}{395}(1.3)^{395}(2.3)^{1105}=1.78\times(10)^{-342} \quad (8)$$

Probability of Edge for √3 :

$$P(X=773)=\binom{1500}{773}(1.3)^{773}(2.3)^{727}=7.42\times(10^{-267}) \quad (9)$$

$$P(X\leq 395)=P(X=1)+P(X=2)+\ldots+P(X=395)$$
$$P(X\geq 773)=P(X=773)+P(X=774)+\ldots+P(X=1500)$$

$$\emptyset\left(\frac{395-E(x)}{\sqrt{V(x)}}\right)\ E(x)=nP=500,\ V(x)=nP(1-P) \quad (10)$$

$$P(X\leq 395)=P(X=1)+P(X=2)+\ldots+P(X=395) \quad (11)$$

$$\emptyset\left(\frac{773-E(x)}{\sqrt{V(x)}}\right)\ E(x)=nP=500,\ V(x)=nP(1-P) \quad (12)$$

$$P(X\geq 773)=P(X=773)+P(X=774)+\ldots+P(X=1500) \quad (13)$$

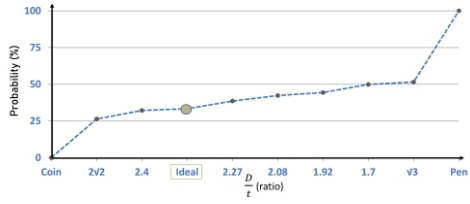

Fig.8: Probability of landing on the side

Table 3: Ratio 2.4 for total number of throws 600

Number of	The results number	The expected number	The difference	percentage
landing on one of its faces	407	400	7	67.83%
landing on its edge	193	200	-7	32.16%
landing on face 1	204	200	4	34%
landing on face 2	203	200	3	33.83%

They brought the results closer to the ideal so not only the geometric characteristics should be considered in this cylindrical dice but the physical properties play important role . There are lots of other physical properties that affects on the outcome of throwing variables like material , initial angular velocity , mass , the angle which the coin is thrown at , friction of the pieces , bounciness and more and the best way to study the effect of each of these variables and get closer than 1.57% to the third probability is a simulation (Fig. 9).

Finding how it works we throw thousands of cylinders while iterating over the cylinders thicknesses then find the thickness at which the coin is equally likely to land on each side then experiment is done a lot of times for different values of different physical properties to find how they affect on the outcome.

Fig.9: Simulation

5. Conclusions

The mass of the cylinder doesn't seem to make a big difference ; it's pretty much steady at a thickness of 0.43 - 0.45 times the diameter . Initial angular velocity shows the more the cylinder spins in the air initially the thicker it has to be it increases between 0.42 and 0.46 (isn't a large difference) (Fig. 10).

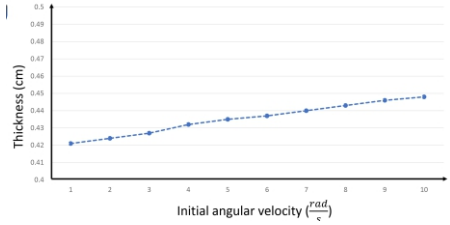

Fig.10: Thickness vs initial angular velocity of dice

The angle which the cylinder is thrown at the surface makes a huge difference ; in this experiment it's the random parameter but I calculated the ratios with different given angles from 90 degrees to 270(Fig. 11) .

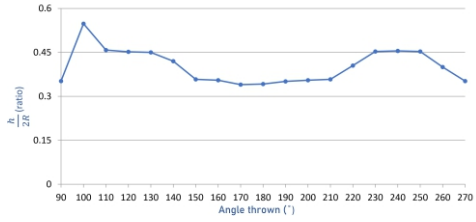

Fig.11: Angle of thrown effect on the results

Friction changes the results a lot and we need a much thicker coin when the coefficient of friction is between 0.1 and 0.18 but after that it decreases (Fig. 12) .

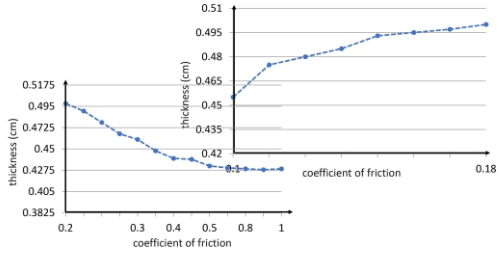

Fig.12: Friction changes on the results

After collecting data with the simulation the best ratio diameter to thickness was found which resulted in exactly third on each face lots of times and generally the probability of it landing on the edge is 2.4655 only 1.23%

further from 33.33% .

The 2.4655 ratio makes the closest to a perfect 3-sided dice but since this is a cylindrical and considering it doesn't have so many symmetry, with exaggerated changes on our physical properties the best cylindrical dice wouldn't be fair anymore so the best 3 sided fair dice would be a cube that has 2 obs 2 twos 2 thres on it.

References

[1] https://ui.adsabs.harvard.edu/abs/1993PhRvE..48.2547M/abstract

[2] https://www.whitman.edu/Documents/Academics/Mathematics/2016/DeHovitz.pdf

[3] https://arxiv.org/pdf/1008.1728.pdf

[4] http://www-groups.mcs.st-andrews.ac.uk/john/

[5] https://www.britannica.com/science/Platonic-solid

[6] https://www.britannica.com/summary/dice

[7] https://en.wikipedia.org/wiki/Dicehttps://arxiv.org/pdf

SYNTHESIS AND DETERMINATION OF DRUG RELEASE BEHAVIORS OF SHAPE MEMORY MAGNETIC NANOCOMPOSITE FILMS

Melek Ceyda Bozan, Balıkesir Şehit ,Prof. Dr. İlhan Varank Bilim ve Sanat Merkezi, melekcebzn@gmail.com

ARTICLE INFO

Gold medalist in BUCA IMSEF 2022

Awarded by Ariaian Young Innovative

Minds Institute , AYIMI

http://www.ayimi.org ,info@ayimi.org

ABSTRACT

Developing efficient drug delivery systems ensure that the drug reaches the target tissue at the highest rate without damaging other tissues. Since magnetic nanoparticles can be controlled externally by magnets, and shape memory polymers can be adapted to any tissue, they are both often used in drug delivery systems. In this study, γ-Fe2O3 nanoparticles and a PVA/regenerated cellulose-cotton solution were combined to develop a more advantageous system that is aimed to be effective to use in target-oriented release of cancer drugs.

Keywords : *Magnetic nanoparticle, Shape memory polymer, Drug release*

1. Introduction

1.1. Polymers

Polymers, also known as macromolecules, are large molecules that are formed by the repetition of one or a group of small chemical units called monomers. The word polymer is formed by the combination of the Latin words “poly” meaning numerous and “meros” meaning piece [22, 23] .

Polymers are divided into three groups according to their chain forms: thermoplastics, elastomers and thermosettings (Fig. 1). Thermoplastics, by means of the linear or branched chains in their structure, can be softened, melted and reshaped by the application of heat. They can be easily dissolved with the use of an appropriate solvent.

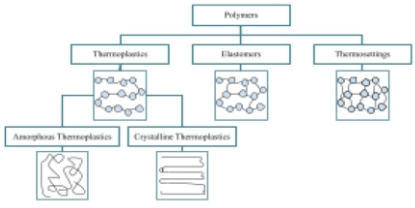

Fig. 1: Classification of polymers depending on the chain structure

The second type of polymers, elastomers which are also known as rubbers, are highly flexible and elastic. Due to the small number of crosslinks between the polymer chains, they can temporarily elongate at a high rate with the tensile effect. The tensile effect causes the polymer chains to slide over each other, but the crosslinks prevent permanent flow, so the molecules return to their original positions when the force is removed.

The third and last type of polymers, thermosettings, are defined as three-dimensional rigid polymers that contain a lot of crosslinks in their structure (network polymers). At high temperatures, they cannot be melted or reshaped, they break down and decompose by breaking the chains and bonds in their structure [19].

Polymeric composites, which are generally obtained from petroleum-derived materials, are materials with a high loading capacity per unit mass, corrosion resistant, easy to process and shape, and suitable for long-term use. There are two types of polymeric composites, the first being thermoset and the second being thermoplastic matrix composites. Thermoset matrix composites are found in liquid form and are first gelled by adding a solidifier and then solidified in order to be shaped. They are frequently used in fibre-reinforced composite making, and during this process, it is often required for them to have a low viscosity. With the effect of heat, can be melted, cooled and solidified, thereby obtaining the ability to be remodeled [11, 12, 16].

1.2. Magnetic Nanoparticles

The word nano means “dwarf” in Greek and denotes one billionth of a unit. Therefore, a nanometer corresponds to one billionth of a meter. Nanostructures are systems consisting of 10-100 atoms, and nanoparticles are nanostructures that are generally between 1-100 nanometers in length [20]. It can be said that there are many subgroups of nanostructures such as nanotubes, nanocrystals, nanowires, nanorods, nanoparticles, and nanofilms. It is seen that nanoparticle production is of great importance for new developments in the field of nanotechnology, owing to its wide application area and superior properties [5, 15].

Nanoparticles could contain materials with different chemical structures such as metals, metal oxides, silicates, organic and carbon materials and biomolecules [17]. The fact that their movements can be easily controlled externally using a magnetic field and their high surface area/volume ratio make magnetic nanoparticles suitable for use in biology, medicine and many more fields, including diagnosis and treatment of numerous diseases, drug delivery, bio-labelling, separation or purification of biomolecules, and medical imaging [3, 24].

Essentially, two approaches are followed for the production of nanoparticles, namely top-down and bottom-up. The top-down approach is based on the separation of the material into nano-sized pieces by energising the volumetric material from the outside by mechanical, chemical or different processes (Fig.2). The bottom-up approach, on the other hand, is the opposite of the top-down approach, aiming to create particles by growing atomic or molecular structures through chemical

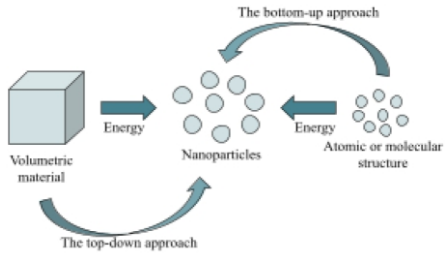

Fig. 2: Procedures used in the production of nanoparticles

One of the main contents of nanoparticles, iron oxides are formed as a result of the chemical combination of iron and oxygen, and approximately 16 types of iron oxide have been identified to date [4]. Since iron oxides, which can be found in many geological and biological processes, are not very sensitive to oxidation, they can maintain the stability of their magnetic effects [20]. Fe_3O_4, α-Fe_2O_3 and γ-Fe_2O_3 are the most common forms of iron oxides in nature. Among these three forms, Fe_3O_4 and γ-Fe_2O_3 nanoparticles have attracted more attention with their superparamagnetic properties, low toxicity, and high surface area/volume ratios. Iron oxide nanoparticles can be used in various biomedical applications such as drug delivery, magnetic resonance imaging (MRI), and protein immobilization, as well as in coating, concrete and paint production [1, 13].

1.3. Smart Materials

Such as diodes and photovoltaics colour or phase-changing, light-emitting piezo materials are defined as smart materials. There are also smart materials that are designed to respond to a stimulating source or that provide optimum interaction by changing the geometry, electromagnetic character and mechanical/physical properties of the molecule [21]. With the current technology, it is possible to produce polymer-based smart materials with different properties that are sensitive to various conditions such as humidity, pH, temperature, light, magnetic field and solvent in the environment [6, 8].

Shape memory polymers, which have the ability to change shape depending on various variables in the environment and then return to their permanent shape, are one of the most frequently used smart polymer types. In recent years, thermosensitive shape memory polymers have been given importance in studies on shape memory polymers due to their wide application area, especially in materials engineering, textile and biomedical devices. In the structure of thermosensitive shape memory polymers, there are often physical or chemical cross-linked points such as various crystals, intertwined chains or amorphous hard segments, which allow their permanent shape to be retained in memory [9].

In addition to their shape memory properties, smart polymers also have the ability to carry about a thousand times their weight. This is due to the high energy released during some property changes. The usability of these polymers, which can easily return to their original shape at body temperature, in the biomedical field is an important research topic. Smart polymers are especially preferred in different biomedical applications such as artificial skin, surgical sutures and drug release. One of the areas where smart biomaterials are frequently used is drug release systems that enable the active substance to be delivered to the target in the body. The sensitivity of smart polymers to properties such as temperature and pH allows the desired change to be made in the desired area of the body, even when a slight difference occurs [21].

2. Method

2.1. Synthesis of Iron (III) Nanoparticles

For this method, after weighing 6.06 and 11.75 grams of ferrous sulfate heptahydrate ($FeSO_4.7H_2O$) and non-hydrated ferric chloride ($FeCl_3$), they were first mixed in 100 mL of distilled water in an ultrasonic environment and then in the ultrasonic water bath without applying heat. 25 mL of 25% ammonium hydroxide solution was added dropwise to the clear solution obtained, and then the resulting precipitated solution was stirred and heated in an ultrasonic environment for 60 minutes. After the resulting brown precipitate was filtered, it was washed with distilled water until pH=7. Afterwards, the precipitate was dried at 70°C for 12 hours and prepared for the analysis [10].

2.2. Preparation of Shape Memory Polymers

In order to prepare the RC-C (regenerated cellulose-cotton) solution, necessary amounts of NaOH, urea and distilled water with a weight ratio of 7:12:81 were used to obtain an aqueous solution in a 250 mL beaker and the resulting solution was cooled. After the cotton, which was previously decomposed in H2SO4, was added to this solution, the solution was mixed vigorously. Then, this solution was centrifuged to remove bubbles and insoluble substances and was taken to a 4°C environment [7, 14] (Fig. 3).

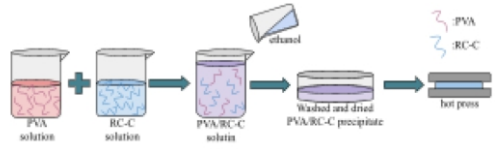

Fig. 3: Preparation of PVA/RC-C composites

The solution consisting of 8 g PVA and 92 g distilled water was heated to 98°C and mixed to obtain 8% by weight PVA solution. Afterwards, the PVA and RC-C solutions were mixed for 30 minutes, and the resulting solution was co-precipitated by adding more ethanol. The precipitate was washed with water, then soaked and dried for several days at 60°C for 4 hours to remove any remaining NaOH and urea. After drying, the PVA/RC-C precipitates were hot pressed at 110°C for 3 minutes [7]. At the end of these processes, γ-Fe_2O_3 nanoparticles were placed into the shape memory polymer at 1%, 2.5% and 5% ratios, and the preparation of shape memory nanocomposite film samples was completed.

2.3. Characterisation of Nanocomposite Films

At this stage, the determination of morphological characteristics of shape memory magnetic nanoparticles were carried out by examining the samples containing 1%, 2.5% and 5% γ-Fe_2O_3 nanoparticles and no nanoparticles with a light microscope.

After that, a dynamic mechanical analyzer was used to analyze the mechanical properties of shape memory magnetic nanocomposites. The tensile strengths of each sample under a force of 1N were calculated.

In order to examine the drug release behaviour of nanocomposite films, a certain amount of samples were transferred into 50 mL buffer solutions, then the solutions were placed in a shaking water bath. Drug release tests lasted for 120 hours in pH=1.2 HCl acid solution and pH=7

phosphate buffer. To determine the amount of clarithromycin released from the nanocomposites, 0.5 mL samples were taken from the solutions per hour and to calculate the concentrations of the samples, absorbance values at 760 nm wavelength were determined and the calibration chart was used [18].

3 Conclusion and Discussion

3.1. Determination of Morphological Characteristics of Shape Memory Magnetic Nanocomposite Films

As a result of the investigations to determine the morphological properties of the prepared nanocomposite films, as shown above, it was seen that the magnetic γ-Fe_2O_3 nanoparticles showed a homogeneous distribution in the shape memory polymer (Fig. 4a-c).

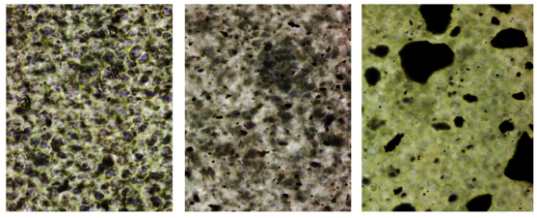

a b c

Fig. 4: Microscopic image of nanocomposite film samples containing a) 1 , b) 2 and c)5 % magnetic nanoparticles, respectively

3.2. Determination of Mechanical Endurance of Shape Memory Magnetic Nanocomposite Films

It is seen that the mechanical endurance of the samples containing nanoparticles is prominently higher than the mechanical endurance of the control sample without magnetic nanoparticles (Table 1). Additionally, it was determined that among the nanocomposite films containing nanoparticles, the sample with the highest mechanical endurance was the sample with 5% nanoparticles, and the sample with the lowest mechanical endurance was the sample with 1% nanoparticles.When the table is examined, it can be seen that the mechanical endurance of the sample with the least amount of nanoparticles increased by 173%, and the sample with the highest amount of nanoparticles increased by 227% compared to the sample without nanoparticles. It was observed that the mechanical endurance of the sample containing 5% nanoparticles reached approximately 3.5 times that of the sample without nanoparticles. The high mechanical endurance ensures that the drug delivery system is not damaged until the drug is delivered to the required tissue, therefore significantly increasing the efficiency of the drug delivery system.

Table 1: The mechanical endurance increase percentage of the samples containing nanoparticles compared to the control sample

Sample	Mechanical Endurance (MPa)	Mechanical Endurance Increase (%)
control	18.38	-
1%	50.15	173%
2.5%	55.86	204%
5%	60.15	227%

3.3. Determination of Drug Release Behaviors of Synthesized Shape Memory Magnetic Nanocomposite Films

It can be easily seen that samples containing nanoparticles have much higher drug loading capacities than the control sample. It was determined that the drug loading capacities of nanoparticle-containing samples are twice the sample without nanoparticles (Table 2) (Fig. 5).

Table 2: Drug loading rates for nanocomposite films with 1%, 2.5% and 5% magnetic nanoparticles

Sample	Drug Loading Rates
control (0%)	48.75%
1%	97.15%
2.5%	99.8%
5%	95.6%

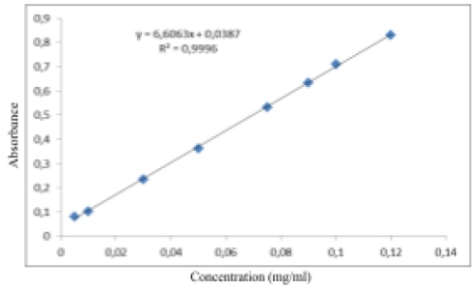

Fig. 5: The standard calibration chart prepared for clarithromycin

In figures (6-9), the drug release amounts of nanocomposite films in the first 10 and 120 hours in environments with pH levels of 1.5 and 7 are given. In both graphs, it is seen that the drug release rates of the samples containing nanoparticles are higher than the samples that do not contain them. Considering that the drug release amounts of the samples containing 5% nanoparticles reached 100% at the end of the 120th hour, it was revealed that the prepared drug release system was more efficient in terms of drug release amount from the shape memory polymer. The fact that the samples containing nanoparticles released at high rates and close to each other in both environments with different pH levels indicate that the synthesised nanocomposite films are compatible with different environments. When the samples containing nanoparticles are compared with each other, it can be concluded that the increase in the nanoparticle ratio will positively affect the drug release, based on the fact that the highest release rate is observed in the sample containing 5% nanoparticles in both samples.

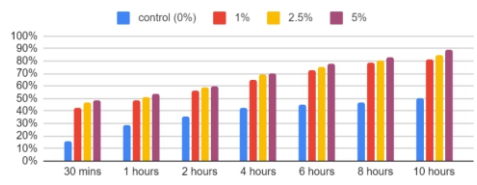

Fig. 6: First 10-hour release graph for pH=1.5

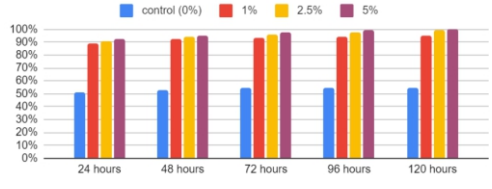

Fig. 7: First 120-hour release graph for pH=1.5

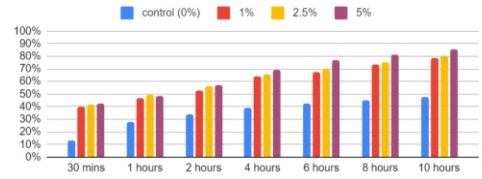

Fig. 8: First 10-hour release graph for pH=7

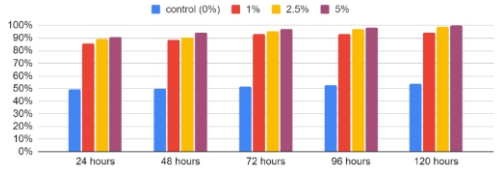

Fig. 9: First 120-hour release graph for pH=7

4. Conclusions

In this study, shape memory magnetic nanocomposite drug carrier polymeric systems, which have not been encountered before in the literature, have been developed. Since it is a fairly new field of study in the scientific world, our study has been very promising in terms of developing new generation drug delivery systems after its biocompatibility has been proven by testing it in cells and tissues in the next stages. Besides, it is known that magnetic nanoparticles have the advantage of being able to control with magnets. It is predicted that the nanocomposite films that we have synthesized using this advantage will be very successful, especially in the controlled and target-oriented direction of cancer drugs. Likewise, since these magnetic nanoparticles are excellent heat conductors after they are delivered to the target tissue, they can be brought to the desired temperature from the outside and used to release the drug at the desired temperature.

References

[1] Başkan, H. (2021). Electrospun composite nanofibers with metal/metal oxide nanoparticles (Doctoral dissertation).

[2] Bottom-up methods for making nanotechnology products. (2018, 16 November). Retrieved from https://www.azonano.com/article.aspx?ArticleID=1079

[3] Chen, F. H., Gao, Q. & Ni, J. Z. (2008). The grafting and release behaviour of doxorubicin from Fe3O4@SiO2 core-shell structure nanoparticles via an acid cleaving amide bond: The potential for magnetic targeting drug delivery. Nanotechnology, 19(16), 1-9. doi: 10.1088/0957-4484/19/16/165103

[4] Cornell R. M. & Schwertmann U. (2003). The iron oxides: Structure, properties, reactions, occurrences and uses. Weinheim, Germany: John Wiley & Sons.

[5] Ebin, B. & Gürmen, S. (2008). Nanopartiküller ve üretim yöntemleri-1 [Nanoparticles and methods of producing them-1]. Metalurji Dergisi, 150, 31-38.

[6] Erdoğuş, H. B. (2019). Biyomedikal uygulamalarda 4B baskı işlemi: Şekil hafızalı malzemelerin katmanlı imalat yöntemiyle üretilmesi [4D printing in biomedical applications: Production of shape memory materials by additive manufacturing method]. International Journal of 3D Printing Technologies and Digital Industry,3(1),86-93.

[7] He, H., Huang, B., Liu, H., Ma, Y., Wu, W. & Zhao, Z. (2019). Mechanically strong, heat-resistant, water-induced shape memory poly (vinyl alcohol)/regenerated cellulose biocomposites via a facile co-precipitation method. Biomacromolecules, 20(10), 3969-3979. doi: 10.1021/acs.biomac.9b01021

[8] Hu, J., Ibekwe, S. I., Li, G. & Meng, H. (2012). A review of stimuli-responsive polymers for smart textile applications. Smart Materials and Structures, 21(5), 1-23. doi: 10.1088/0964-1726/21/5/053001

[9] Kaplan, S. & Korkmaz Memiş, N. (2018). Şekil hafızalı polimerler ve tekstil uygulamaları [Shape memory polymers and textile applications]. Tekstil ve Mühendis, 25(111), 264-283. doi: 10.7216/1300759920182511111

[10] Kasap, S. & Kaya, İ. İ. (2018). γ-Fe2O3 Nanoparçacık katkılı üç boyutlu grafen köpüklerin üretimi ve karakterizasyonu [Fabrication and characterization of γ-Fe2O3 doped three dimensional graphene foam]. Dokuz Eylül Üniversitesi Mühendislik Fakültesi Fen ve Mühendislik Dergisi, 20(60), 743-754. doi: 10.21205/deufmd. 2018206058

[11] Kaya, A. İ. (2015). Atık kâğıtlardan geri kazanılmış liflerden kompozit malzeme üretim olanaklarının araştırılması [Investigation of composite material production possibilities from recycled fibers from waste paper] (Doctoral dissertation).

[12] Kaya, A. İ. (2016). Kompozit malzemeler ve özellikleri [Composite materials and their properties]. Putech & Composite Poliüretan ve Kompozit Sanayi Dergisi, 29, 38-45.

[13] Koh, P. Y. & Teja, A. S. (2009). Synthesis, properties, and applications of magnetic iron oxide nanoparticles. Progress In Crystal Growth and Characterization of Materials, 55(1-2), 22-45. doi: 10.1016/j.pcrysgrow.2008.08.003

[14] Li, R., Lu, A., Wang, S. & Zhang, L. (2015). Dissolution of cellulose from different sources in a NaOH/urea aqueous system at low temperature. Cellulose, 22, 339-349. doi: 10.1007/s10570-014-0542-6

[15] Liveri, V. T. (2006). Controlled synthesis of nanoparticles in microheterogeneous systems. New York, NY: Springer Science & Business Media.

[16] Morozov, E. & Vasiliev, V. V. (2001). Mechanics and analysis of composite materials. Oxford, England: Elsevier Publications.

[17] Pekdemir, M. E. (2011). Manyetik nanopartiküller kullanılarak yüzeyde güçlendirilmiş raman spektrometrisi ile immunoassay sisteminin geliştirilmesi [Development of magnetic nanoparticle based ımmunoassay system via surface enhanced raman spectroscopy] (Master's thesis).

[18] Polat, S. (2020). Antikanser ilaçların kontrollü salımı için pektin bazlı sıcaklık/pH/manyetik alan duyarlı nanopartikül sentezi ve karakterizasyonu [Synthesis and characterization of pectin based temperature/ ph/ magnetic field sensitive nanoparticle for controlled anticancer drugs] (Master's thesis).

[19] Saçak, M. (1998). Polimer kimyasına giriş [Introduction to polymer chemistry]. Ankara, Turkey: A.Ü.F.F. Döner Sermaye İşletmesi Yayınları.

[20] Sarıbuğa, S. (2014). Manyetik nanopartiküllerin analitik incelenmesi [The analytical examination of the magnetic nanoparticles] (Doctoral dissertation).

[21] Tüylek, Z. (2019). Sağlık alanında kullanılan akıllı polimerler [Smart polymers used in the field of health]. İnönü Üniversitesi Sağlık Hizmetleri Meslek Yüksek Okulu Dergisi, 7(1), 81-95. doi:

ALLOMETRY

Setareh Sabeti, Farzanegan 2 high School, Tehran, Iran

ARTICLE INFO

Participated in PYNT 2017

Advisor: Dr. Mohammad Qorbani

Accepted by Ariaian Young Innovative Minds Institute , AYIMI

http://www.ayimi.org ,info@ayimi.org

ABSTRACT

If we want to create a new creature (by stimulation of new stem cells), we should apply allometric scaling and equations in designing processes. For example, if the target be the creation of a human, her/his skull should become approximately twofold after the puberty period. Allometry helps us to guess the size of different parts of the body in different ages that is how the doctors find out how much our stature will grow. Here, we show the allometric scaling of different kind of animals which shows a logarithmic behaviors.

Keywords : *Stem Cell, Allometry, animals, logarithmic*

1. Introduction

It is clear that the body of animals and humans is made of different parts and organs. These parts and organs grow during time gradually and everything about the biology of an animal is influenced by its body size, including its physiology (e.g., heartrate, respiratory rate, total metabolic rate, mass specific metabolic rate, growth rate), anatomy (e.g., organ mass, blood volume, surface area, cross-sectional area of limbs), and ecology (e.g., diet, home range size, reproductive strategy, life span, population density) [1]. But the question is that "what happens to these different parts when an animal grows?" and to answer this question many tries have been done [2]. There are many researches which show when the body becomes more massive, different parts become larger. These studies are the subjects of allometry science. Hence, Allometry is the study of how these processes scale with size of the body. In its broadest sense, it describes how the characteristics of living creatures change with size. The term originally referred to the scaling relationship between the size of a body part and the size of the body as a whole, as both grow during development. However, more recently the meaning of the term allometry has been modified and expanded to refer to biological scaling relationships in general. In this research, we searched to find the charts that shows how much the different important parts of the human body (such as bones, brain and heart) or body of animals (such as legs, antennae or horns) relate to each other [1]. One of the most general concepts that you are likely to find in biology is that of the relationship between body size and the rest of an organism's biology, a relationship that is often referred to as allometry. Therefore, an exploration of this topic is important if we are to understand the relationship between form and function in vertebrates. The purpose of learning allometry study is to explore for ourselves the relationship between two important biological traits: volume (a function of mass) and surface area, and how this relationship influences other aspects of an animal's biology. Allometry literally means "of other or different measures" (allo = other or different; metry =measure). The goal of its study with respect to biology is to describe the differences in magnitude in form or function that are correlated with changes in form or function of another variable [3].

2. Experiment

Allometry does not have any direct experiment. Therefore, the only thing that we should do is: search and read the gathered data in the libraries, websites and published papers. We've also investigated the documents about the dinosaurs in museums and national parks and got information about allometry equation. We've also investigated allometric scaling in different parts of different animals bodies. We realized that allometry is not always additive for example Our heads are almost a quarter of our body size when we are born, but when we grow to become adults our heads are only 1/8 or so (or heads grow slower than the rest of our body) and it is negative allometry (Fig. 1).

We found it ourselves by investigating the table of height, weight and height and weight of head growing during gestational period.

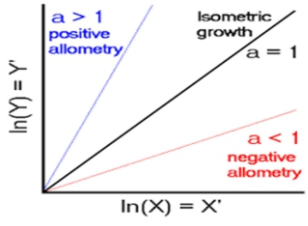

Fig. 1: The chart which shows negative and positive allometry[5].

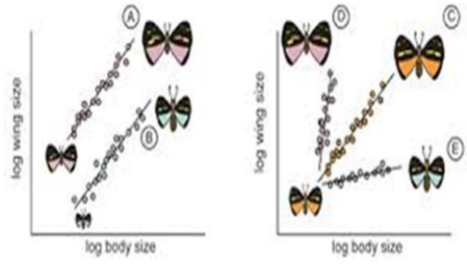

Fig. 2 : Allometric scaling of butterfly wings [1]

We also found many charts about allometric scaling of different parts of the body of different animals (Figs. 2 to 5) and Table (1).

Table. 1: Mass and length of a baby inside the mothers [3]

getational age	length(us) (crown to rump)	weigt(us) (crown to rump)	length(cm)	mass(g)
8weeks	0.63inch	0.04 ounce	1.6	1
9weeks	0.90inch	0.07 ounce	2.3	2
10weeks	1.22 inch	0.14 ounce	3.1	4
11weeks	1.61inch	0.25 ounce	4.1	7
12weeks	2.13inches	0.49 ounce	5.4	14
13weeks	2.91 inches	0.81 ounce	7.4	23
14weeks	3.42 inches	1.52 ounce	8.7	43
15weeks	3.98 inches	2.47 ounces	10.1	70
16weeks	4.57 inches	3.53 ounces	11.6	100
17weeks	5.12 inches	4.94 ounces	13	140
18weeks	5.59 inches	6.70ounces	14.2	190
19weeks	6.02 inches	8.47ounces	15.3	240
20weeks	6.46 inches	10.58ounces	16.4	300
21weeks	10.08 inches	10.58ounces	25.6	300
22weeks	10.51 inches	12.70ounces	26.7	360
23weeks	10.94 inches	15.17ounces	27.8	430
24weeks	11.38 inches	1.10 pound	28.9	501
25weeks	11.81 inches	1.32 pound	30	600
26weeks	13.62 inches	1.46 pound	34.6	660
26weeks	14.02 inches	1.68 pound	35.6	760
27weeks	14.41 inches	1.93 pound	36.6	875
28weeks	14.80 inches	2.22pounds	37.6	1005
29weeks	15.2 inches	2.54pounds	38.6	1153
30weeks	15.71 inches	2.91pounds	39.9	1319
31weeks	16.18 inches	3.31pounds	41.1	1502
32weeks	16.69 inches	3.75pounds	42.4	1702
33weeks	17.20 inches	4.23pounds	43.7	1918
34weeks	17.72 inches	4.73pounds	45	2146
35weeks	18.19 inches	5.25pounds	46.2	2383
36weeks	18.66 inches	5.78pounds	47.4	2622
37weeks	19.13 inches	6.30 pounds	48.6	2859
38weeks	19.61 inches	6.80 pounds	49.8	3083
39weeks	19.96 inches	7.25 pounds	50.7	3288
40weeks	20.16 inches	7. 63pounds	51.2	3462
41weeks	20.35 inches	7.93pounds	51.7	3597
42weeks	20.28 inches	8. 12pounds	51.5	3685

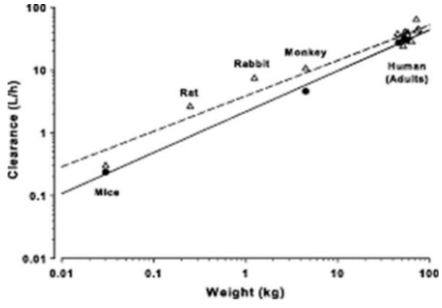

Fig. 3 : Information of different animals and human [5]

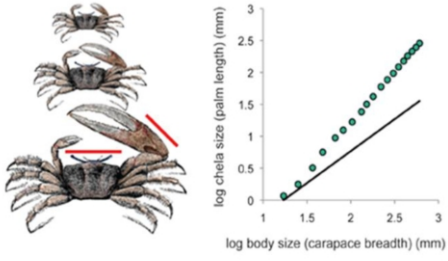

Fig. 4: Allometric scaling of chela and carapace of crab [1].

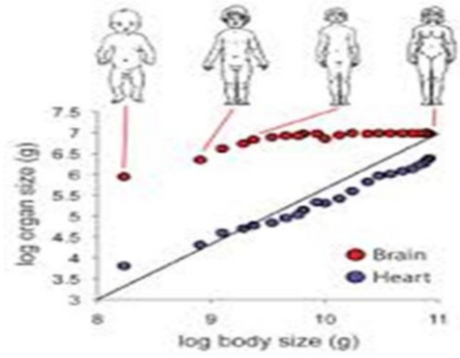

Fig. 5: Allometric scaling of brain and heart of humans [1]

3. Results

More simply, it is the study of what happens to Variable Y when you change Variable X. This is basically a qualitative description and only allows us to speak of correlated changes in qualitative ways; for example, Y gets bigger as X gets bigger, Y slows down as X speeds up, Y gets wider as X gets heavier, and so on. As biologists, however, we want to be able to describe things in a more precise way.

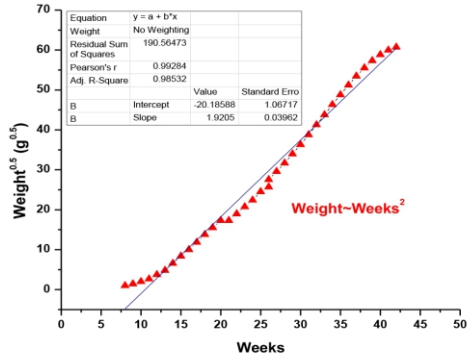

Fig. 6 : Chart of weight growing during time (OUR MODELING)

Does Y get bigger (or slow down or get wider) at the same rate as X? At a faster rate? A slower rate? To satisfy our need for quantification, we resort to mathematical equations that precisely describe the relationship between two variables. We investigated the table of humans head growing during gestational period* and found out my own equations. We've also drawn the charts of these information ourselves (Figs. 6 to 9).

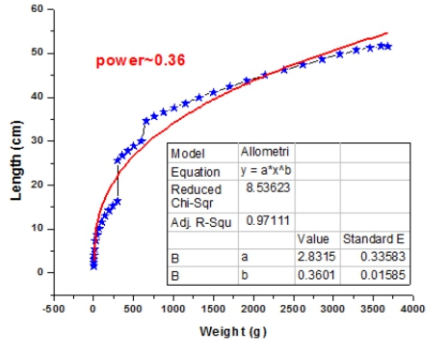

Fig. 7 : chart of length growing relating to the weight (OUR MODELING)

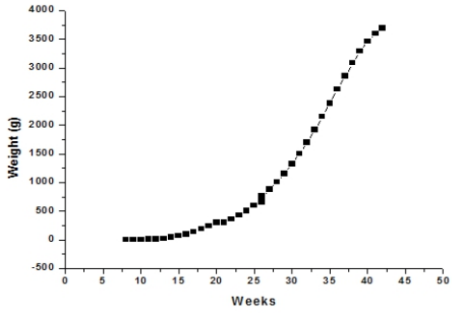

Fig. 8: Chart of weight growing during time (OUR MODELING)

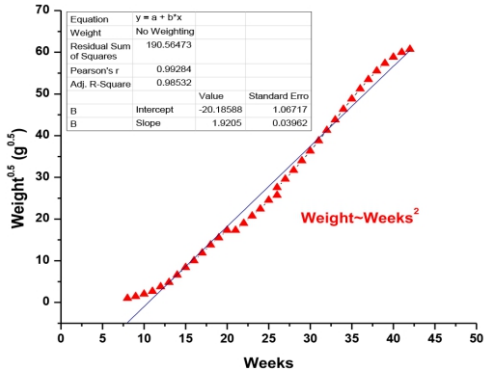

Fig. 9: Chart of (weight)^(0.5) growing during time

4. Conclusion

Allometry scaling shows that when an animal or human grows up, different parts of its body become larger and all of these parts grow relating to the whole body size. We are not always able to measure the size of different parts of the body such as inner parts like brain or heart and we can figure it out by the allometric equations that describe the relationships between two variables(like weight of the whole body and length of the crown in humans). Allometry is not always positive and it's sometimes (like humans head) negative when a particular part of the body grows slower than the rest of the parts.

References

[1] https://www.nature.com

[2] R. Lande, Quantitative Genetic Analysis of Multivariate Evolution, Applied to Brain: Body, Evolution, 33, 1979, 402-406.

[3] Allometry in Biological Systems, Stephen C. Trombulak, Department of Biology, Middlebury College

[4] http://www.babycenter.com

[5] https://www.mun.ca

[6] http://www.iynt.org

[7] https://www.aac.asm.org

[8] http://www.wikipedia.com

COLORED FIRE

Mohammad Erfan Nadeali, Andisheh Farda School, Mashhad, Iran, erfannadali670@gmail.com

ARTICLE INFO

Participated in IYNT 2022, Georgia

Advisors: Reza Rasekh, Hamidreza Faghani

Accepted by Ariaian Young Innovative

Minds Institute , AYIMI

http://www.ayimi.org ,info@ayimi.org

ABSTRACT

The flame can be easily painted using different chemicals. To identify the chemicals needed to obtain a particular color and check what color is obtained if a combination of these chemicals are used, several experiments have been done. All colored flames with different chemical substances are captured to compare with each other.

Keywords : *Flame, Chemical Substances, colored Fire*

1. Introduction

Are electrons excited by heat? Electrons can also be excited by electrical excitation, where the original electron absorbs the energy of another, energetic electron. The simplest method is to heat the sample to a high temperature. The thermal energy produces collisions between the sample atoms causing the atom's electrons to be excited.

When an electron in an atom has absorbed energy it is said to be in an excited state. An excited atom is unstable and tends to rearrange itself to return to its lowest energy state. When this happens, the electrons lose some or all of the excess energy by emitting light (Fig. 1).

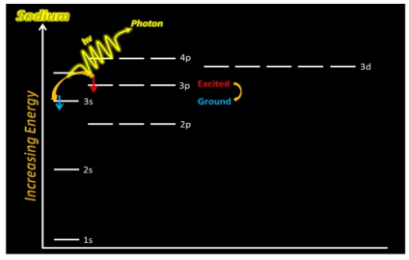

http://ircamera.as.arizona.edu/Astr2016/lectures/spectroscopy.htm

Fig. 1: Radiation from excited atom

2. The Origin of Flame's Colors

We should know that the color of each flame is determined by the temperature of the material is used .

The temperature ranges from Red to White:

Red

Just visible: 525 °C (980 °F)
Dull: 700 °C (1,300 °F)
Cherry, dull: 800 °C (1,500 °F)
Cherry, full: 900 °C (1,700 °F)
Cherry, clear: 1,000 °C (1,800 °F

Orange

Deep: 1,100 °C (2,000 °F)
Clear: 1,200 °C (2,200 °F)

White

Whitish: 1,300 °C (2,400 °F)
Bright: 1,400 °C (2,600 °F)
Dazzling: 1,500 °C (2,700 °F)

As shown ,the lower the color temperature is and the warmer more reddish the color of the light will be and the higher the color temperature is the cooler more bluish the color of the light will be.

The white light source with a high proportion of red and a low color temperature will appear warmer.

The white light source with a high proportion of blue and a higher color temperature will appear cooler.

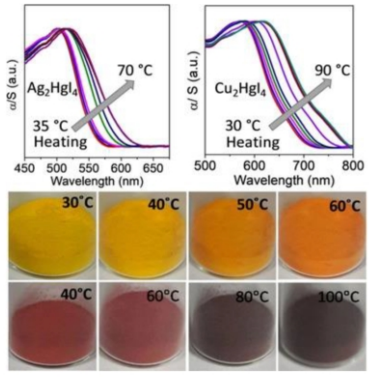

Fig. 2: The concepts of color temperature

3. Materials and Methods

All materials in this research are in Table (1).

Table 1: Chemical substances in our experiments

Material	Chemical Formula	color
1-Magnesium sulfate	$MgSO_4$	White
2-Potassium chloride	KCl	White
3-Copper chloride	$CuCl_2$	Green
4-Boric acid	H_3BO_3	White
5-Copper sulfate	$CuSO_4$	Blue
6-calcium chloride	$CaCl_2$	White
7-Strontium chloride	$SrCl_2$	White
8-Barium chloride	$BaCl_2$	White

4. Experiment

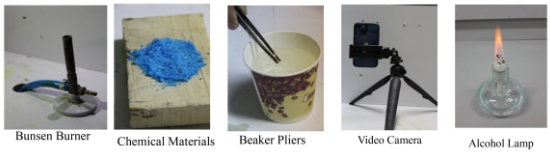

Fig. 3: Experimental Setup

All experiments have been done with different chemical substances and the flame's colors are observed in Bunsen burner and Alcohol lamp.

Flame's Color of Magnasium sulfate , $MgSo4$, is Blue and KCl is Purple, $CuCl_2$ is Green and boric acid flame's Color is light green so $CuSo_4$ flame's Color is Green also $CaCl_2$ flame's Color is Orange and $SrCl_2$ is Red.

Experiments are compared in different temperatures (Fig. 4).

Fig. 4: Flame's color with different chemical substances

Experiment with combined substances reslted in new color which depends on percentage of mixture of each substances. Combining the 33% manuseim solfate + 66% boric asid and making blue and green color is one of the experiments but the green color is more than the blue color because the percentage of boric acid is more than that of magnesium sulfate. Measuring the temperature of materials with a laser thermometer is recorded.

The results of all materials in my tests are in Table (2).

Table 2: The results

Material	Chemical Formula	Material color	Real color	Observed color	Bunsen Burner Flame temperature	Alcohol lamp Flame temperature	color temperature	Wavelength
1-Magnesium sulfate	$MgSO_4$	White	Blue	Blue	1500°C	260°C	1400 ~ 1500°C	450 ~ 495
2-Potassium chloride	KCl	White	Purple	Purple	1500°C	260°C	1200 ~ 1400°C	380 ~ 450
3-Copper chloride	$CuCl_2$	Green	dark green	dark green	1500°C	260°C	1400 ~ 1600°C	495 ~ 570
4-Boric acid	H_3BO_3	White	light green	light green	1500°C	260°C	1400 ~ 1600°C	495 ~ 570
5-Copper sulfate	$CuSO_4$	Blue	Green	Green	1500°C	260°C	1400 ~ 1600°C	495 ~ 570
6-calcium chloride	$CaCl_2$	White	Orange	Orange	1500°C	260°C	1000 ~ 1200°C	590 ~ 620
7-Strontium chloride	$SrCl_2$	White	Red	Red	1500°C	260°C	800 ~ 1000°C	620 ~ 750
8-Barium chloride	$BaCl_2$	White	light purple	light purple	1500°C	260°C	1200 ~ 1400°C	380 ~ 450

5. Conclusion

Different types of substances were tested to find temperatures and the excitation of materials on different flames. The best visible spectrum was on the Banzen Burner because it had a high flame temperature. But in the alcohol lamp, because the flame temperature was very low, the substances couldn't excite well and the visible spectrum was not produced as well as the Banzen-Burner.

References

[1] Yigithan Dedeoglu, B. Ugur Töreyin, Ugur Cidikbay, A. Enis CelinBilkent University, TR-06800 Bilkent, Ankara, TurkeyREAL-TIME FIRE AND FLAME DETECTION IN VIDEO

[2] Automatic quantification of colour proportions in dorsal black-and-yellow coloured amphibians, tested on the fire salamander (Salamandra salamandra) Eugenia Sanchez1,*, Sven Gippner1 , Miguel Vences1 , Kathleen Preißler1 , Isabelle J. Hermanski2 , Barbara A. Caspers2 , E. Tobias Krause3 , Sebastian Steinfartz1 and Friedrich-Wilhelm Kastrup

[3] Fredholm theory for the mean first-passage time of integrate-and-fire oscillators with colored noise input

[4] Carl van Vreeswijk and Farzad Farkhooi Phys. Rev. E **100**, 060402(R) – Published 17 December 2019

DISEASE DETECTION FROM CHICKEN FECES ON A MOBILE PLATFORM USING DEEP LEARNING METHODS

Akbudak, Burak Sina , Turkey, buraksinaakbudak@gmail.com

ARTICLE INFO

Gold medalist in BUCA IMSEF 2022

Awarded by Ariaian Young Innovative

Minds Institute , AYIMI

http://www.ayimi.org ,info@ayimi.org

ABSTRACT

The demand for poultry, which has been an important economic activity for humanity for thousands of years, is increasing due to many reasons . One of the most important factors that negatively affect poultry farming is pathogenic animal diseases. The detection of diseases in poultry is usually done through laboratory tests, the disease progresses and causes mortality in the time required for laboratory examinations. In this study, a mobile application was developed to minimize the mentioned problems and to enable poultry producers to obtain fast and reliable information about diseases that occur in their animals.

Keywords : *Chicken diseases, Deep learning, Mobile application.*

1. Introduction

In this study, a mobile application was developed to minimize the mentioned problems and to enable poultry producers to obtain fast and reliable information about diseases that occur in their animals. To be used in this mobile application, a deep learning model has been developed that can distinguish pseudo-plague (Newcastle strain), salmonella, and coccidiosis diseases in chicken feces through the data collected by processing the photographs taken from the feces of chickens with the help of tools such as artificial intelligence, machine learning, and image processing, which are widely used today. To train the deep learning model used, a dataset of 6812 photos consisting of chicken droppings was prepared for training deep learning models and models previously used for various purposes were trained through transfer learning. After the training, the models were evaluated comparatively and the model with the highest accuracy and efficiency ratio was selected for use in the mobile application. In addition, a panel has been developed in which users can get information about possible diseases that may be found in their chickens as a result of answering questions about the symptoms that can be observed in their chickens.

Poultry farming, which has been shown as one of the main economic activities of humanity for thousands of years, gains importance every year due to the advantages it provides for producers and consumers, and as a rapidly growing economic sector on a global scale, it is closely related to a large part of the world's population. Poultry farming, which stands out as an economic activity with a high-profit margin due to the competitive advantage that can be achieved even at local scales due to the low opportunity cost for the producers, is also frequently preferred by consumers due to its high nutritional value and relatively more economical conditions. Considering these reasons, it is seen that the demand for poultry farming is already increasing at exponential levels all over the world, and it is predicted that this trend will gradually accelerate in the future as well. So much so that since 1995, the demand for chicken meat in the world has doubled every 10 years; the egg and other poultry products market has achieved a growth of around one hundred and fifty percent on a global scale [2]. At the same time, the waste and other by-products generated after production are rich in elements such as nitrogen, phosphorus, calcium, and potassium that are necessary for soil quality and will increase product yield, a chicken produces 5 kilograms of waste that can be used as fertilizer annually, chemical agents rapidly pollute the currently limited resources. and due to reasons such as commercial fertilizers do not produce sustainable solutions for ecological balance, the poultry farming sector; gains a position that directly or indirectly affects the basic economic activities in many countries. In particular, the use of chicken manure in agricultural activities is expanding in Asia Minor and many African countries such as Pakistan, and Iran, where access to chemical fertilizers and reinforcing agents is limited [3].

As a sector that affects the entire food web in the ecosystem, poultry farming, like all other livestock sectors, is critically adversely affected by emerging animal diseases. As in many countries of the world, these diseases are viewed as the most important obstacle to sectoral development and competitiveness for Turkey. Although the breeders in Turkey do not have difficulty in reaching a certain quality in the final products to be exported, they lose their potential export opportunities due to widespread zoonosis and animal diseases and there are economic losses that will deeply affect the sector [1]. In addition, poultry diseases transmitted to other foods and water sources through agricultural processes in which the wastes produced by chickens are used as fertilizer pose a high danger to public health, especially to the people living in rural areas. Considering that poultry farming is in a more complex relationship with other economic activities, especially in developing countries where access to health services and protective measures is relatively inadequate, it is seen that this situation constitutes a major deficiency in terms of preventing epidemics that are currently on the agenda of the whole world. So much so that typhoid fever, which is a common chicken disease and a disease caused by Salmonella bacteria, has lost its power in countries such as the USA, Denmark, and Turkey, where the sanitary infrastructure has developed since the 2000s, but only in the border regions of Pakistan and Iran in 2017-2018. It has caused the death of hundreds of people by developing new mutations with a high mortality rate and antibiotic

resistance even within the range [4].

In addition to diseases caused by bacteria, viral infections transmitted from poultry to humans also cause major problems both locally and globally. Avian Influenza, which is known as "bird flu" among people, has deeply affected many countries, including Turkey, in the 2000s. In addition to new viruses such as H7N9, which are currently circulating in countries such as China, Vietnam, and Thailand and can be transmitted from person to person [5], studies conducted in Western and Sub-Saharan Africa regions draw attention to a new H5N1 danger [6]. Considering the incurable viruses such as HIV, which can transmit from other vertebrates to humans through mutations, and SARS-CoV-2, which has been affecting the whole world for more than 2 years, biosecurity is of high importance today, and solutions that can detect pathogenic diseases of poultry origin at the earliest and the lowest cost are considered. It is seen that the need is increasing day by day. Considering the damage caused by many poultry diseases to the intestinal and digestive tracts, it is thought that chicken droppings may be a good indicator for the most common poultry diseases such as coccidiosis (coccidiosis), pseudo-plague (Newcastle strain) and Salmonella-related diseases.

Coccidiosis, which is a deadly disease seen in many vertebrates due to protozoa of the Eimeria genus, adversely affects the intestinal tract of the infected creature and causes problems such as tissue damage, diarrhea, decreased resistance to other diseases, and in some cases death [7]. Coccidiosis disease causes great harm to the poultry industry, considering the negative effects on animals that die due to the disease and producers who come into contact with live, feces, and other wastes. So much so that, according to 2016 data, coccidiosis caused a loss of over £100 million in the UK alone; It has been found to cause damage to the poultry farming industry in developing countries such as Brazil, Egypt, Guatemala, India, and Nigeria at a level of over £10 billion that could be classified as devastating [8].

Although drugs and vaccines have been developed for the prevention and early diagnosis of coccidiosis disease, due to the high cost of drugs and the logistical barriers to establishing the necessary infrastructure for widespread vaccination in developing countries, they could not be easily made available to poultry producers, prompting the producers to seek more natural, economical and effective solutions. [9].

Newcastle strain (false plague), another common poultry disease in the world, is reported as a deadly and contagious disease affecting many domestic and wild animal species. The only known diagnostic method for the diagnosis of this disease, which is seen in Asia, Africa, and parts of North and South America, is high-cost and long-term laboratory tests. Many producers do not seek medical help except in very urgent cases due to the high cost, even though symptoms are observed and the disease is suspected, and this situation endangers public health as well as causes financial damage. Another dangerous situation related to pseudo-plague is that it is a disease with a high ability to cross-transmission between species. For this reason, vaccine makers and laboratory workers are the most affected by the Newcastle strain, which can infect bird species as well as spread among humans, and resistant mutations that are more difficult to treat can be seen. [10]

Salmonella-based diseases have been followed as an international public health threat since the 2000s, as a disease with high mortality. According to 2015 data, Salmonella bacteria, which causes 93.8 million food-borne diseases and 155,000 annual deaths [11], continues to be effective in many countries, especially in African countries, East Asia, and Asia Minor, although it has lost its effect in countries such as Turkey and European countries [12]. Salmonella Enterica, one of more than 2000 different serotypes, tends to cause systemic diseases in humans. Although progress has been made in the fight against Salmonella with today's technology, the immunity of pathogens against the substances used and the fact that it is a pathogen that can be transmitted to humans through food makes a full-scale control in poultry difficult without effective early diagnosis methods [13]. This situation causes great economic damage to the chicken farming sector.

As one of the biggest common points of poultry diseases, which are pregnant with such great economic problems and cause harm to the ecological balance, changes in the appearance of chicken droppings can be shown due to the effects of diseases on the digestive system [14]. In particular, detecting the apparent differences in stools with the help of computer vision algorithms, which have recently played a role in the detection of many diseases and problems, will be able to eliminate the logistical impossibilities and cost problems, which are one of the most fundamental problems in the diagnosis of diseases. Today, computer vision technologies are used in quite different fields such as health [15], agriculture [16], and livestock [17]; It is used for purposes such as image classification, image recognition, and image segmentation. To perform the image classification process used in this study, firstly, the images to be classified are named with appropriate classes, and a data set is created. Then, a deep learning model, which is thought to be suitable, is trained with this data set and a model trained on that data set is obtained. This model is tested by using the test set separated from the data set before the training process and the accuracy of the model is obtained. For example, the working group led by Ranjbarzadeh [18] developed a deep learning model that can segment brain tumor images with an accuracy of 92%, and Konstantinos P. Ferentinos [19] identified 58 different plant diseases with an accuracy of 99.53%. has developed a deep-learning model that can diagnose.

As one of the biggest common points of poultry diseases, which are pregnant with such great economic problems and cause harm to the ecological balance, changes in the appearance of chicken droppings can be shown due to the effects of diseases on the digestive system [14]. In particular, detecting the apparent differences in stools with the help of computer vision algorithms, which have recently played a role in the detection of many diseases and problems, will be able to eliminate the logistical impossibilities and cost problems, which are one of the most fundamental problems in the diagnosis of diseases. Today, computer vision technologies are used in quite different fields such as health [15], agriculture [16], and livestock [17]; It is used for purposes such as image classification, image recognition, and image segmentation. To perform the image classification process used in this study, firstly, the images to be classified are named with appropriate classes, and a data set is created. Then, a deep learning model, which is thought to be suitable, is trained with this dataset and a model trained on that dataset is obtained. This model is tested by using the test set

separated from the data set before the training process and the accuracy of the model is obtained. For example, the working group led by Ranjbarzadeh [18] developed a deep learning model that can segment brain tumor images with an accuracy of 92%, and Konstantinos P. Ferentinos [19] identified 58 different plant diseases with an accuracy of 99.53%. has developed a deep-learning model .

2. Method

Deep learning algorithms, which are a sub-field of machine learning algorithms, can reach very high accuracy rates in areas of use such as classification, object detection, and segmentation in computer vision. Deep learning algorithms, which use artificial neural networks created by imitating the cognitive process of humans, are widely used in the construction of autonomous vehicles, the development of chatbots, and image processing. Although artificial intelligence networks used in deep learning have a convolutional neural network (CNN), generative contentious network (GAN), recursive neural network (RNN), and similar network structures, each is used by researchers in line with different requirements. In this study, we have used the CNN structure, which enables deep learning to transform images into digital matrices.

In line with the aforementioned purposes, (i) a suitable development environment has been established in the computer environment, (ii) operations have been made on the dataset, (iii) appropriate deep learning models have been trained, and (iv) a mobile application has been developed to ensure that the work done is accessible to all segments.

A. Creating the Development Environment

One of the issues that the researcher should decide before starting any artificial intelligence study is to choose the artificial intelligence software framework to be used. Tensorflow and PyTorch are the most popular artificial intelligence and deep learning frameworks used worldwide today. The Keras API, which works on these software frameworks and facilitates their use, is widely used in today's deep learning research. In this research, it was decided to work with the TensorFlow software framework using the Python software language, due to a large number of users in the world and the rapid application development. After the software framework has been determined, it has been deemed appropriate to work with the Conda package manager to use different versions of the libraries at the same time, to make experiments, and to provide environmental management easily.

In the first stage, artificial neural networks were run on the CPU to make the experiments, but with the growth of the data set, the use of GPU, which is hardware that can run more than one process in parallel, was needed. For this, the first artificial intelligence models were created with the NVIDIA GTX 1650Ti GPU, and GPU acceleration processes were configured using the NVIDIA CUDA Toolkit. Due to the growth of the network architectures used in artificial intelligence models to reach higher accuracy values and the limited video memory (VRAM) of the GPU used accordingly, the Google Colaboratory, which is offered to researchers free of charge, has been switched to the Colab platform. The Colab notebook, which is accessed through the browser, allows the codes written using the Python programming language to run in the cells it contains. Colab offers access to GPUs in servers located in data centers for free with no extra configuration required for use in machine learning. In this study, it has been actively used and the power of the hardware in the data centers has been used in training artificial intelligence models.

B. Applied Operations on the Dataset

The dataset contains a total of 6812 photographs, of which 2057 are healthy, 2103 are coccidiosis, 376 are Newcastle strains, and 2276 are salmonella disease. Some of these photos were collected by us using the ODK (Open Data Kit) mobile application. ODK is a mobile application that allows quick tagging of photos taken while taking a photo. Data were collected and labeled under the supervision of a veterinarian from a small poultry farm (Fig.1).

Fig. 1: Data Collection and Labeling Using ODK Application

The photos in the dataset are of different resolutions because they were taken by different mobile phone cameras. However, the requirement that all photos fed to the artificial intelligence model must be of the same resolution (for example, 299 pixels x 299 pixels) necessitated the application of intelligent cropping and resizing to each photograph. While doing this, attention was paid to the aspect-width ratio and the value of the data was tried to be preserved as much as possible. Examples of data are shown in Figure (2).

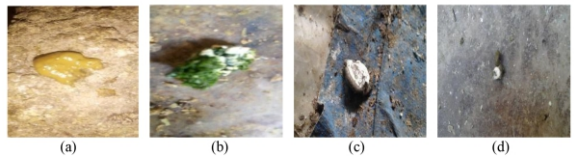

(a) (b) (c) (d)

Fig.2: Examples of Data (a) Coccidiosis (b) Newcastle Strain (c) Healthy (d) Salmonella

The data duplication method, which is another of the preprocessing methods applied to the data set, was used both to increase the number of high-quality data to be fed to the model and to avoid the problem of data imbalance between classes, which is one of the factors affecting the performance of the model.

Table 1: Duplication Operation on Dataset

Classes	Number of Data Before Duplication	Number of Data After Duplication
Healthy	2057	4114
Coccidiosis	2103	4206
Newcastle Strain	376	2256
Salmonella	2276	4552
Total	6812	15128

In the data duplication process, techniques such as random enlargement, vertical or horizontal rotation of the photo, random amount of zoom in/out, and a random

amount of clockwise/counterclockwise rotation were applied to each photo, and the number of photos in the dataset increased to 15128. However, more replication was performed in Newcastle Strain disease, which has fewer data than other diseases and causes an imbalance between classes, compared to other classes. Since it would cause poor quality of data in the Newcastle strain class, which reached almost half the number of other classes, no further replication was performed and the imbalance problem between classes, which was the first step towards a solution after preprocessing, was solved during the training phase of the model. The results of this duplication process are shown in Table 1. At the same time, examples of photographs formed after duplication are shown in Figure (3).

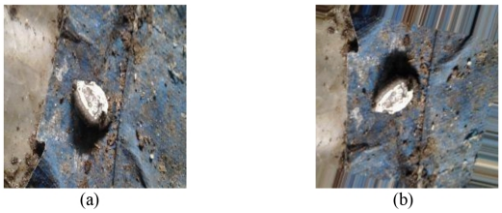

(a) (b)

Fig.3: Salmonella Class Data Before (a) and (b) After Replication Process

After duplication, the dataset was divided into 3 parts (80%-10%-10%) for (i) training, (ii) testing, and (iii) validation of the model. The results of this separation process are shown in Table(2).

Table 2: Segmentation of the Dataset into Training-Test-Validation Parts

Classes	Training	Test	Validation
Healthy	3291	411	411
Coccidiosis	3365	421	421
Newcastle Strain	1804	226	226
Salmonella	3642	455	455
Total	10899	1363	1363

C. Training the Deep Learning Models

To feed the data set to the network, which is the first stage of training deep learning models, a software pipeline should be established. The tf.data module in TensorFlow has been preferred to be used for importing the data set due to its high speed and easy application. In other data input generation modules, while the artificial neural networks wait for the data to be processed first and then enter the network, the tf.data data processing module divides the data set into data stacks and queues them in the RAM region, and feeds the incoming data stacks to the network. This module, which is 38 times faster than other data entry creation modules, benefits from the advantages of parallel processing.

After the data set is transferred to the program, before the data set is divided into training and test parts, the problem of imbalance between classes still needs to be resolved in the results obtained by preprocessing. To overcome this problem, it was decided to use the class weights method. The class weights method ensures that certain weights are assigned to each class during the training of the model and that classes with a small number of data in the back-propagation process affect the model more, thus preventing the accuracy rate decreases, which are caused by the unequal distribution of the classes in the data set and especially affecting the F1-score.

Research has been carried out on which network architecture can be used by the artificial intelligence models that will be created when the data set is ready to be fed to artificial neural networks as a training and test set after the preprocessing processes. The performance levels of network architectures achieved in previous studies were examined and studies were started to create models from prominent architectures. While some of the most advanced architectures are readily available within the Keras API, the architectures used to make the first trials were built manually from scratch using object-oriented programming techniques, again over the Keras API. Some of the readily available architectures can be seen in Table 4. The first 1 accuracy rate and top 5 accuracy rate columns are the performance data obtained by testing the model trained using the specified architecture on the ImageNet dataset. Depth refers to how many layers the network has topologically, such as the activation layer, the batch normalization layer, the pooling layer, and similar layers.

Table 3: Data on Different Deep Learning Models

Model	Size (MB)	Top 1 Accuracy Rate	Top 5 Accuracy Rate	Number of Parameters	Depth
Xception	88	0.790	0.945	22,910,480	126
VGG16	528	0.713	0.901	138,357,544	23
VGG19	549	0.713	0.900	143,667,240	26
ResNet152	232	0.766	0.931	60,419,944	-
InceptionV3	92	0.779	0.937	23,851,784	159
MobileNet	16	0.704	0.895	4,253,864	88
MobileNetV2	14	0.713	0.901	3,538,984	88
DenseNet201	80	0.773	0.936	20,242,984	201

Our work in this research started with Mini VGGNet, which uses fewer resources and has lower complexity than advanced architectures. MiniVGGNet;It is an architectural structure inspired by the VGGNet [23]architectural family, with much less complexity than the architectures in the VGGNet architecture family. As the studies progressed, it was decided to increase the complexity of the architecture to increase the accuracy of the model on the data set and to reach a model structure that can generalize real-world scenarios. At the end of the study, considering the mobile application to be developed, Xception[24], which is very popular today, VGG16 from the VGG architecture family, MobileNetV2[25], and Resnet 50[26] optimized for mobile, each model has been started to be trained to compare each model.

The VGGNet architecture, which won the 2014 ImageNet competition, outperformed its predecessors by using a 3x3 Convolution Filter consisting of 16 or 19 layers. Developed by François Chollet, the designer of the Keras deep learning library, Xception is inspired by the Inception architecture. While standard convolutional layers perform spatial computation in one step, depth-wise separable convolution divides the computation into two steps. Developed by Mark Sandler and his colleagues in 2019, MobileNetV2 outperformed many of its predecessors produced for mobile use, taking the state of the art one step further using existing popular datasets. The Resnet architecture, developed by Kaiming He and his colleagues, which won the ImageNet competition in 2015,

has been designed to have much less complexity, although it uses 8 times more layers than the VGGNet architecture family.

Transfer learning, another method used with the architectures mentioned above, is a method developed to take the features learned in a problem and use them on a new problem. In this study, previously learned features of different classes were transferred to the models developed by the transfer learning method by using the models created on the ImageNet data set.

Hyperparameters are various parameters that are adjusted according to certain rules and trial-and-error methods when training deep learning models.

Table 4: Hyper Parameters Used in Training the Deep Learning Model

Parameters	Value
Learning Rate	0.0001
Epoch Number	20
Batch size	32
Optimization Algorithm	SGD

The explanations of the parameters mentioned in Table 4 are given below:

(i) Learning Rate: This parameter determines how much the weights of the model will change depending on the margin of error.

(ii) Epoch Number: This parameter determines how many times a data batch (batch) will be learned by the model.

(iii) Batch size: This parameter determines how much data will be learned by the model in each round.

(iv) Optimization Algorithm: This parameter determines which optimization algorithm will be used during the training of the model. Among the most used optimization algorithms, SGD (Stochastic Gradient Descent)[27], Adam[28], and Adagrad [29] can be given.

The sample hyperparameters used for this research took their final form as shown in Table 4 after various attempts were made to train the models. Finally, the training of the models was carried out using the GPU in the Colab notebook.

Table 5: Data on Training Different Deep Learning Models on the Created Dataset

Models	Training Accuracy	Validation Accuracy	F1 Score
Xception	0.93	0.88	0.91
VGG16	0.76	0.72	0.7
MobileNetV2	0.85	0.83	0.82
Resnet 50	0.74	0.66	0.69

The statistical evaluations (Table 5) obtained after the models were trained were compared. Even if the Xception network structure has reached the highest accuracy rate, since the model will work on the mobile device, the MobileNetV2 network structure, which is a more optimized model for working on the mobile device, has been preferred.

D. Mobile Application Development

It has been decided to develop a mobile application so that everyone can benefit from the artificial intelligence models obtained as a result of the studies. Necessary optimizations have been made to enable the artificial intelligence model to work on mobile so that every person with an Android smartphone can analyze whether there is a disease in their chicken.

Flutter is used for the development of the mobile application of this project; It is an open-source UI software development kit created by Google. It uses the Dart programming language created by Google for mobile and web development purposes. Among the reasons for deciding to use the Flutter mobile development kit in this project are Flutter's open-source code, its speed compared to its peers, its ability to easily design impressive interfaces, and its detailed and explanatory documentation. After the decision to use the Flutter mobile development kit, the Flutter development environment was established and the general design of the mobile application was made. Using the TensorFlowLite library, which was developed to use the trained deep learning models in the mobile application, the deep learning model with the best results was optimized and made ready for use in the mobile application.

With the increase in information and data, different methods were needed to store data. One of these methods is databases. Databases work according to the principle of putting the data that wants to be stored in the appropriate row and column under a table. In this study, a database that can only be used for reading (no data transfer from the application to the database), does not need any network connection, and can run on a local device is needed. The necessary literature review was made and it was seen that the SQLite database met the desired features so it was decided to use the SQLite database in the mobile application. Using SQL (Structured Query Language) language, SQLite is an open-source SQL database engine that can be used in many different languages and does not need an external server, that is, can run on a local device. In this study, the SQLite database was used to store information about diagnosed diseases. In this way, diseases added to the database in the future, and their explanations will be able to be used without any changes in the code of the mobile application.

Users who open the mobile application encounter the first page called the "Home Page", where the diagnosis of diseases can be made as "Diagnostics by Photo" or "Diagnostics with Questions" (Figure 4(a)). When the user clicks the "Diagnose with Photograph" button, on the page titled "Diagnose with Photograph" (Figure 4(b)), the user is expected to enter a photo via gallery or camera. The result obtained by processing the input given to the system by the deep learning model is “Click here for information about the disease.” On the page titled “Information Page” (Figure 4(c)), which can be accessed with the help of the button, the name of the disease, the symptoms of the disease, the actions to be taken against the disease, and general information about the disease are examined under 4 headings.

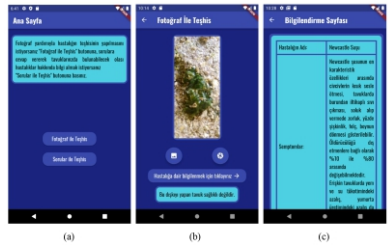

Fig. 4: Screenshots of Mobile Application While Working on Android Virtual Device (a) Home Page, (b) Diagnosis by Photo, (c) Part of Information Page

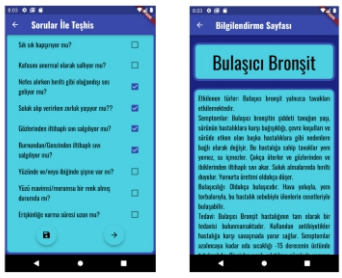

(a) (b)

Fig. 5: (a) Diagnosis with Questions, (b) Part of the Information Sheet

When the user clicks on the "Diagnostic with Questions" button on the page titled "Home Page", he will be greeted with the questions directed to him on a page titled "Diagnostic with Questions" (Fig. 5a). After giving the necessary answers to the questions, they should record their answers. After clicking on the Save button and clicking on the button to go to the next page, the page titled "Information Page" (Fig. 5b), you will see information about possible diseases/diseases that can be seen in your chickens.

3. Results

After obtaining the necessary data and performing "duplication" and clipping operations on the data, a data set that can be used for training the models was obtained (Table 1). Then, the obtained dataset was divided into 3 parts training-test-verification (Table 2). The models were trained with the parameters specified in Table 3 on the created dataset. Although XceptionNet performed better among the deep learning models that were trained, the MobileNetV2 model, which can work more optimized in the mobile application, was found suitable for the use of the mobile application to be developed (Table 5) and it was made ready to be integrated into the mobile application with the help of the TensorflowLite library. Then, two panels of the mobile application, "Diagnostic by Photo" and "Diagnose with Questions" were developed. After the integration of the database and deep learning model into these panels, the user-friendly interface of the mobile application was improved and the mobile application became ready.

4. Conclusion and Discussion

When the accuracy rates obtained from the trained models were examined, it was seen that the 82% accuracy rate obtained for disease detection from the feces of chickens was suitable for use in the mobile application, and the MobileNetV2 model, which will work in the most optimized way in the mobile application, was integrated into the mobile application after the necessary preparations. Then, the "Diagnostics with Questions" panel of the mobile application was developed, and a connection was established with the database of the mobile application to display information to the user in line with the received data.

5. Suggestions

While doing this study, it was considered that the dataset and database could be expanded with different diseases in the following stages, and the structures created were established to serve this purpose. Therefore, by training different deep learning model structures through the new dataset obtained by expanding the dataset, a higher accuracy rate than the models obtained in this study can be obtained and the newly trained model can be used in the developed mobile application. In addition, the number of questions in the "Diagnosis with Questions" panel of the mobile application can be increased and the database containing data on diseases can be expanded by adding new diseases.

References

[1] Robyn Alders, Rosa Costa, Rodrigo A. Gallardo, Nick Sparks, Huaijun Zhou,Smallholder Poultry: Leveraging for Sustainable Food and Nutrition Security, Editor(s): Pasquale Ferranti, Elliot M. Berry, Jock R. Anderson, Encyclopedia of Food Security and Sustainability, Elsevier, 2019, Pages 340-346, ISBN 9780128126882, https://doi.org/10.1016/B978-0-08-100596-5.21544-8.

[2] Scanes, C G. Poultry Science, (Jun 2007): 1057-8. access address: https://www.proquest.com /openview/1f603cfeecfd0b5e5683dddfad40d27d/1?cbl=48306&parentSessionId=QyNPcK%2BIHODBqnlpkZlUA%2Fs3j5Rf6VpfGnKhElEir8k%3D&pq-origsite=gscholar

[3] Muhammad Aamer Maqsood, Naqsh-e-Zuhra, Imran Ashraf, Nasir Rasheed, Zia-ul-Hassan Shah, Chapter 2 - Sources of nitrogen for crop growth: Pakistan's case, Editor(s): Tariq Aziz, Abdul Wakeel, Muhammad Arif Watto, Muhammad Sanaullah, Muhammad Aamer Maqsood, Aysha Kiran, Nitrogen Assessment, Academic Press, 2022, Pages 13-28, ISBN 9780128244173, https://doi.org/10.1016/B978-0-12-824417-3.00005-8.

[4] Herekar, F., Sarfaraz, S., Imran, M., Ghouri, N., Shahid, S., & Mahesar, M. (2021). Clinical spectrum and outcomes of patients with different resistance patterns of Salmonella enterica. Pakistan Journal of Medical Sciences ©. 38, Issue ICON-2022). Pakistan Journal of Medical Sciences. https://doi.org/10.12669/pjms.38.icon-2022.5789

[5] Chen, Y., Bai, T., & Shu, Y. (2022). Poultry to Human Passport: Cross-species Transmission of Zoonotic H7N9 Avian Influenza Virus to Humans. Zoonoses (C. 2, Issue 1). Compuscript, Ltd. https://doi.org/10.15212/zoonoses-2021-0026

[6] Shaban, S., Kyei, F., Awuni, J., Danquah, A., Odoom, T., Yingar, D. N. Y. T., Ababio, P. T., & Emikpe, B. O. (2021). Dynamics of influenza A (avian influenza) virus in poultry in the Greater Accra region of Ghana amongst the production levels. Journal of Immunoassay and Immunochemistry (C. 43, Issue 1). Informa UK Limited. https://doi.org/10.1080/15321819.2021.1952426

[7] El-Shall, N. A., Abd El-Hack, M. E., Albaqami, N. M., Khafaga, A. F., Taha, A. E., Swelum, A. A., El-Saadony, M. T., Salem, H. M., El-Tahan, A. M., AbuQamar, S. F., El-Tarabily, K. A., & Elbestawy, A. R. (2022). Phytochemical control of poultry coccidiosis: a review. Poultry Science (C. 101, Issue 1, s. 101542). Elsevier BV. https://doi.org/10.1016/j.psj.2021.101542

[8] Blake, D. P., Knox, J., Dehaeck, B., Huntington, B., Rathinam, T., Ravipati, V., Ayoade, S., Gilbert, W., Adebambo, A. O., Jatau, I. D., Raman, M., Parker, D., Rushton, J., & Tomley, F. M. (2020). Re-calculating the cost of coccidiosis in chickens. Veterinary Research ©. 51, Issue 1). Springer Science and Business Media LLC. https://doi.org/10.1186/s13567-020-00837-2

[9] M. De Gussem, Coccidiosis in poultry: review on diagnosis, control, prevention and interaction with overall gut health, access address: https://www.cabi.org/isc/FullTextPDF/2009/20093257328.pdf

[10] Abdisa, T., & Tagesu, T. (2017). Review on Newcastle Disease of Poultry and its Public Health Importance. Journal of Veterinary Science & Technology (C. 08, Issue 03). OMICS Publishing Group. https://doi.org/10.4172/2157-7579.1000441

[11] Eng, S.-K., Pusparajah, P., Ab Mutalib, N.-S., Ser, H.-L., Chan, K.-G., & Lee, L.-H. (2015). Salmonella: A review on pathogenesis, epidemiology and antibiotic resistance. Frontiers in Life Science (C. 8, Issue 3, ss. 284-293). Informa UK Limited. https://doi.org/10.1080/21553769.2015.1051243

[12] Marchello, C. S., Carr, S. D., & Crump, J. A. (2020). A Systematic Review on Antimicrobial Resistance among Salmonella Typhi Worldwide. The American Journal of Tropical Medicine and Hygiene (C. 103, Issue 6, ss. 2518-2527). American Society of Tropical Medicine and Hygiene. https://doi.org/10.4269/ajtmh.20-0258

[13] Chiu, C.-H., Su, L.-H., & Chu, C. (2004). Salmonella enterica Serotype Choleraesuis: Epidemiology, Pathogenesis, Clinical Disease, and Treatment. Içinde Clinical Microbiology Reviews (C. 17, Issue 2, ss. 311-322). American Society for Microbiology. https://doi.org/10.1128/cmr.17.2.311-322.2004

[14] Y. M. Saif, Diseases of Poultry, 2008, Editörler: A.M. Fadly, J.R. Glisson, L.R. McDougald, L.K. Nolan, D.E. Swayne

[15] Srinivasu, P. N., SivaSai, J. G., Ijaz, M. F., Bhoi, A. K., Kim, W., & Kang, J. J. (2021). Classification of Skin Disease Using Deep Learning Neural Networks with MobileNet V2 and LSTM. Içinde Sensors (C. 21, Issue 8, s. 2852). MDPI AG. https://doi.org/10.3390/s21082852

[16] M. Arivukarasi and A. Antonidoss, "Performance Analysis of Malicious URL Detection by using RNN and LSTM," 2020 Fourth International Conference on Computing Methodologies and Communication (ICCMC), 2020, pp. 454-458, doi: 10.1109/ICCMC48092.2020.ICCMC-00085.

[17] Ms. Saily Kini, Mr. Saurabh Hadpe, Mr. Vishal Rasal, Prof. Janhavi Sangoi, "Comparative Study on Advanced Farm Security System Using Internet of Things and Image Processing.", VIVA-IJRI Volume 1, Issue 4, Article 70, pp. 1-7, 2021. Published by Computer Engineering Department, VIVA Institute of Technology, Virar, India.

[18] Ranjbarzadeh, R., Bagherian Kasgari, A., Jafarzadeh Ghoushchi, S., Anari, S., Naseri, M., & Bendechache, M. (2021). Brain tumor segmentation based on deep learning and an attention mechanism using MRI multi-modalities brain images. Içinde Scientific Reports (C. 11, Issue 1). Springer Science and Business Media LLC. https://doi.org/10.1038/s41598-021-90428-8

[19] Ferentinos, K. P. (2018). Deep learning models for plant disease detection and diagnosis. Içinde Computers and Electronics in Agriculture (C. 145, ss. 311-318). Elsevier BV. https://doi.org/10.1016/j.compag.2018.01.009

[20] Bao, Y., Lu, H., Zhao, Q., Yang, Z., & Xu, W. (2021). Detection system of dead and sick chickens in large scale farms based on artificial intelligence. Içinde Mathematical Biosciences and Engineering (C. 18, Issue 5, ss. 6117-6135). American Institute of Mathematical Sciences (AIMS). https://doi.org/10.3934/mbe.2021306

[21] Zhuang, X., Bi, M., Guo, J., Wu, S., & Zhang, T. (2018). Development of an early warning algorithm to detect sick broilers. Içinde Computers and Electronics in Agriculture (C. 144, ss. 102-113). Elsevier BV. https://doi.org/10.1016/j.compag.2017.11.032

[22] Mbelwa, H., Mbelwa, J., & Machuve, D. (2021). Deep Convolutional Neural Network for Chicken Diseases Detection. Içinde International Journal of Advanced Computer Science and Applications (C. 12, Issue 2). The Science and Information Organization. https://doi.org/10.14569/ijacsa.2021.0120295

[23] K. Simonyan and A. Zisserman, "Very deep convolutional networks forlarge-scale image recognition," arXiv 1409.1556, 09 2014

[24] F. Chollet, Xception: Deep learning with depthwise separable convolutions, 2017, access address: https://arxiv.org/abs/1610.02357

[25] Mark Sandler and Andrew Howard and Menglong Zhu and Andrey Zhmoginov and Liang-Chieh Chen, 2019, access address: arXiv:1801.04381

[26] K. He, X. Zhang, S. Ren, and J. Sun, Deep residual learning for image recognition, 2015, access address: arXiv:1512.03385

[27] Zhang, Sixin and Choromanska, Anna E and LeCun, Yann. Deep learning with Elastic Averaging SGD, 2015 Editörler: C. Cortes and N. Lawrence and D. Lee and M. Sugiyama and R. Garnett

[28] Diederik P. Kingma, Jimmy Ba. Adam: A Method for Stochastic Optimization, 2017, access address: arXiv:1412.6980

[29] A. Agnes Lydia, F. Sagayaraj Francis, Adagrad - An Optimizer for Stochastic Gradient Descent, 2019, access address: http://ijics.com/gallery/92-may-1260.pdf

FLOATING OF A METAL DISK ON THE WATER SURFACE

Kiana kamali poorshiraz , Farzanegan 2 high school, Tehran, Iran, kiana.k83@gmail.com

ARTICLE INFO

Participated in PYPT, IYPT 2022

Advisor: Alireza Noroozshad

Accepted in country selection by Ariaian Young Innovative Minds Institute , AYIMI

http://www.ayimi.org ,info@ayimi.org

ABSTRACT

When a metal disk is placed in a vessel of water it shall sink due to its higher density but the water jet impinges on the center of the disk may cause it to be floated . The hydraulic jump is formed in the edges of the disk by the water jet that passes radially away from the center of the disk to the edges. This jump causes a difference in the level of the height above and under the disk which will increases pressure under the disk. Water above the disk is moving with higher velocity compared its velocity to water under the disk so due to Bernoulli's principle, the pressure difference between them increases. pressure difference and then minimum velocity of the water jet.

Keywords : *Metal disk, Hydraulic jump, Water jet, Stability*

1. Introduction

In this research a metal disk in a vessel of water is studied. A metal disk with a hole at its center sinks in a container filled with water. when a vertical water jet hits the center of the disk , it may float on the surface. It shall sink due to its higher density but as an external force here the water jet impinges on the center of the disk and it is observed that the disk floats.To find relevant parameters several experiments are designed with qualitative analysis.

2. Theories and Methods

In the beginning there are two possibilities:

1- The radius of the water jet is smaller than the radius of the whole so the whole flow of the water jet passes through the hole.

2- In the second scenario radius of the water jet is bigger than the radius of the hole so that there is a flux of water passing radially away from the center.

Since the first case will not keep every metal disk floated we will observe the second scenario in more details (Figs.1 & 2).

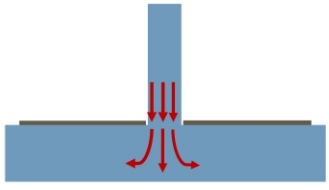

Fig. 1: The whole flow of water passes through the hole

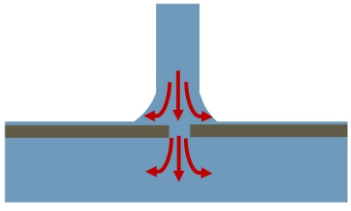

Fig. 2: Part of water flows radially away from the center to edges on the disk

To illustrate forces acting on our disk there is a free body diagram. Gravity force is pulling our disk downward then as the water jet impinges to the center there is an extra force acting downward but still we see our disk stays floated so there must be an upward force acting against our downward forces that prevent our disk from sinking now we want to find the origin and minimum amount of this upward force (Fig. 3).

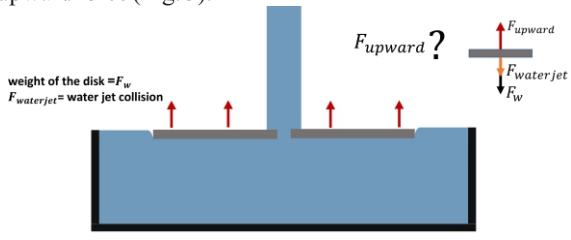

Fig. 3: Forces are applied on the disk

Before moving on to the theoretical framework there are some concepts that we need to understand. First hydraulic jump which as our jet impinges to the center of the disk it flows radially away from the center to the edges with higher velocity and makes the super critical flow then at the edges of our disk there is a jump formed with this super critical flow which collides with the subcritical flow with less velocity. To observe characteristics of this jump we defined two Froude number one refers to outer film depth being outer Froude number and one refers to inner film depth as inner Froude number (Figs. 4 &5) (Eqs. 1-3).

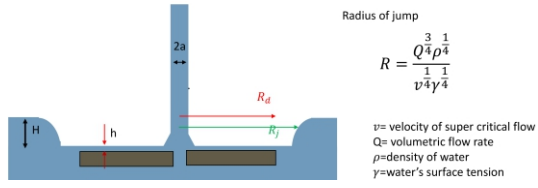

Fig. 4: Hydraulic jump and its radius

Froude number :

$$F_{ro} = \frac{Q}{2\pi R_j \sqrt{gH^3}} \quad (1)$$

$$F_{ri} = \frac{\lambda Q}{2\pi R_j \sqrt{gh^3}} \quad (2)$$

Fr_o = outer Froude number based on outer film depth
Fr_i = Froude number based on inner film depth

$$H = \left(\frac{-1+\sqrt{1+8Fr_i^2}}{2}\right)h \tag{3}$$

Since the velocity of the thin layer of water above the disk is not uniform and constant we have a correction factor to be calculated also the height of the jump can be measured by using inner Froude number and depth of water inside the jump. There is a circular hydraulic jump in this phenomenon, radius of the jump can also be calculated proportional to velocity of super critical flow, volumetric flow rate, density of water and surface tension (Eq. 4) .

Since system is in equilibrium $\Rightarrow \Sigma F = 0$

$F_{downward} = F_{mg} + F_j$

$F_{up} = F_p$

$F_p = F_w + F_j$

$$F_j = \rho Q v \tag{4}$$
$$F_w = mg$$

By Newton's second law and equation of momentum the water jet force is calculated but we have to note that the volumetric flow rate is not the whole water coming out of water jet. To have a better approach, there is an approximate illustration of the water jet . Two fluxes in the edges represented by red collide with the disk and the flux of water in the middle represented by green passes from the center of the hole (Fig. 5) (Eqs. 5&6).

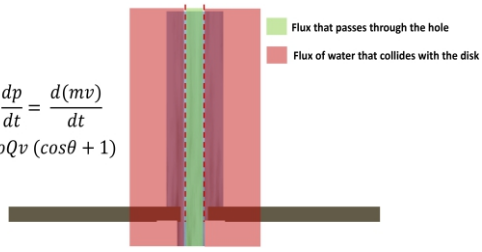

$$F = \frac{dp}{dt} = \frac{d(mv)}{dt} \tag{5}$$

$$F_j = \rho Q v\,(cos\theta + 1) \tag{6}$$

Fig. 5: Flux passes through or collide the disk

The other concept is Bernoulli's principle, when the water jet impinges to the center there is a part of water moving above the disk with higher velocity compared to the velocity of water under the disk leads to a difference in pressure above and under it and by higher pressure under the disk there is an upward force (Eq. 7).

Dynamic Pressure

$$p_1 + \frac{1}{2}\rho v_1^2 + \rho g h_1 = p_2 + \frac{1}{2}\rho v_2^2 + \rho g h_2 + Lp \tag{7}$$

Static Pressure

$v_1 > v_2$, $P_1 < P_2$ → Higher pressure under the disk → F_{upward}

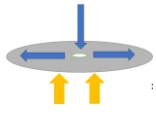

Since our system is in equilibrium sum of all forces should equal to zero , downward forces of weight of the disk and water jet force. Upward force is caused by the difference in pressure which minimum amount of this force can be measured . On the other hand, there is another way to calculate this upward force which is multiplying the difference in pressure to the area of the disk in order to do that we have to find the difference in pressure above and under our disk (Fig.6) (Eq.8).

Using Bernoulli's principle that p_1 stands for pressure under the disk and p_2 stands for pressure above it and since the velocity of water under the disk is almost zero that component will be omitted also the height of water above the disk is negligible so that component would also be omitted lastly we can find the difference in pressure as this equation.

$F_p = mg + \rho Q v$

Pressure under the disk

$$p_1 + \cancel{0} + \rho g h_1 = p_2 + \frac{1}{2}\rho v_2^2 + 0 \tag{8}$$

Pressure above the disk

on the other hand $F_p = \Delta P A$

Therefore : $\Delta P = \frac{1}{2}\rho v^2 - \rho g h$

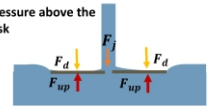

Fig. 6: Forces applied on the disk

Thickness of the thin layer of water above the disk should be measured to find characteristics of hydraulic jump and due to Watson's determination we defined Reynold's number and proportion of radius of the disk to the radius of the water jet and found this equation to calculate the thickness of thin layer but we still have to find the velocity of non-uniform film of water above the disk (Eq.9) (Fig. 7) .

$$Re = \frac{2Q}{\pi a v}, \quad \frac{R_d}{a} = 0.366 Re^{\frac{1}{3}} \Rightarrow h = \frac{2\pi^2 v(R_j^3 + 0.286 a^3 Re)}{3\sqrt{3}\, Q R_j} \tag{9}$$

R_d = radius of the disk
a = radius of the jet
v = velocity of jet

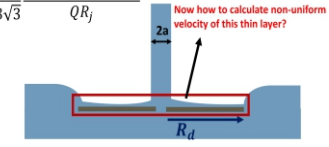

Fig. 7: Non-uniform velocity of the thin layer

Going back to the inner Froude number that we defined here we need to find the correction factor which by integrating from the velocity of the thin layer of water the equation above and by applying the boundary conditions final we can define the Froude number and due to Watson's solution we defined a delta here which represent the proportion of vertical location relative to the surface which Watson gave a solution to find the correction factor (Eqs.10-13).

$$F_{ri} = \frac{\lambda Q}{2\pi R_j \sqrt{g h^3}} \quad (\lambda \text{ is the correction factor}) \tag{10}$$

Inner Froude number can be written as :

$$F_{ri} = \frac{\sqrt{\frac{1}{h}\int_0^h u^2 dz}}{\sqrt{gh}} \tag{11}$$

If $u = f u_{z=h}$, $R_j > R_d$ and $Q = 2\pi R_j \int_0^h u dz$

$$F_{ri} = \left(\frac{\sqrt{\int_0^1 f^2 d\delta}}{\int_0^1 f d\delta}\right)\frac{Q}{2\pi R_j \sqrt{gh^3}} \tag{12}$$

u= velocity of thin film
Z= vertical location relative to surface

$\delta = \frac{z}{h} = 1$ (free-surface of inner film)

Watson also suggested a solution $\Rightarrow c\delta = \int_0^f (1 - x^3)^{-0.5} dx$

$\Rightarrow c = 1.4$

If $R_j > R_d$; $f(1) = 1$, $f(0) = 0$ ($boundary\ condition$)

The correction factor :

$$\lambda = \frac{\sqrt{\int_0^1 f^2 d\delta}}{\int_0^1 f d\delta} = \frac{3c^{\frac{3}{2}}}{\sqrt{2\pi}} = 1.12 \tag{13}$$

3. Experiment

A supply tank with an adjustable nozzle was used and water jet impinged to the center of various disks which for experimental data we varied radius of the water jet, radius of the hole, mass of the disk, radius of the disk and also the existence of hole in the center and for all experiments distance between nozzle and disk were constant .

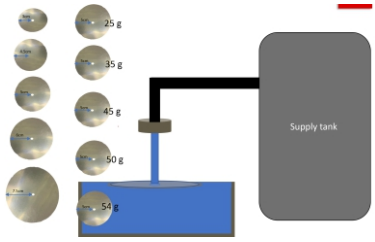

Fig. 8: Experimental Setup

4. Results

By analyzing the data it is observed as the radius of the disk increases the minimum velocity that was necessary for the disk to stay floated would also increase similarly. As the disk gets heavier minimum velocity of the water jet would also increase (Figs. 9&10).

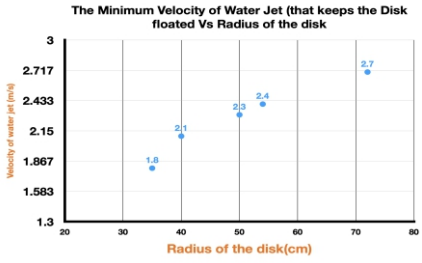

Fig. 9: The velocity of water jet versus radius of the disk

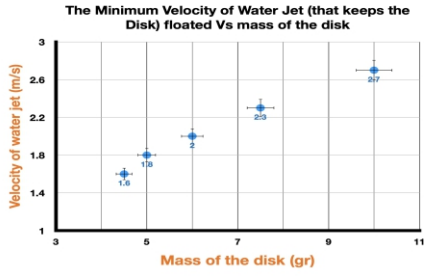

Fig. 10: The velocity of water jet versus mass of the disk

A color-coded chart is used to find how the proportion of radius of the disk and radius of the hole affect on the phenomenon qualitatively which the best floating was possible when the radius of water jet was bigger than the radius of the hole (Fig.11).

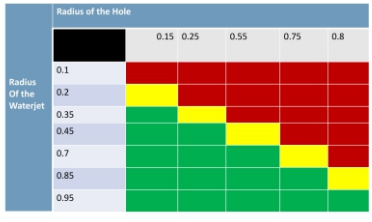

Fig. 11: Color-coded chart in analyzing data

Another color-coded chart is used to show how increasing each parameter changes the floating of the disk which green represents stable floating, yellow stands for floating with oscillation and red stands for sinking (Fig. 12).

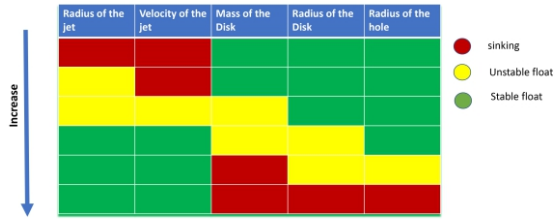

Fig. 12: Another color-coded chart in analyzing data

The next thing in our experiment was simulating the disk and impingement of water jet on the disk with and without the hole. In both cases hydraulic jump was observed but what is the reason that we don't see floating of a disk without the hole in the center (Fig. 13)?

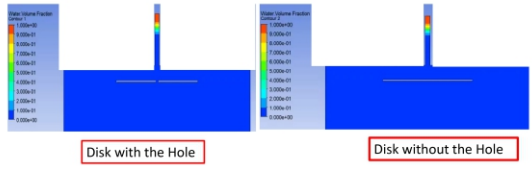

Fig. 13: Simulation results

we even tried to investigate this experimental that the disk with a dent in the center is floated in stable position but for the disk without the hole floating was possible in the beginning but within less than a second it started sinking. Because when the water jet is applied to a disk without any dent on the surface the reaction force is vertically upward and since the disk is placed in water it can move horizontally away but for the second case that has a dent in the center , the reaction force from the edges of that dent can be divided to its x and y components which x components cancel each other and that is the reason that our water jet stays in the center and floating is stable.

By comparing the theory with experimental data we found the force caused by the difference in pressure in two ways and by putting them as equals, also the minimum velocity of the water jet that each disk needs in order to be floated .

5. Conclusions

The relation between minimum velocity and radius/mass of the disk also the radius of the hole in the center of the disk are found by the experiments.

The fact that upward force which is keeping our disk floated is mainly due to Bernoulli and hydraulic jump. The hole in the center of the disk works as a system stabilizer.

In order to see this phenomenon, radius of the water jet must be bigger than the radius of the hole in the center. The first scenario that we suggested only works for very light disks. By equations minimum velocity of the water jet that keeps our disk floated was calculated too.

References

[1] Alexis Duchesne, Anders Andersen and Tomas Bohr, Surface tension and the origin of the circular hydraulic jump in a thin liquid film, Department of Physics, Technical University of Denmark.

[2] Semat, Henry and Katz, Robert, "Physics, Chapter 9

Hydrodynamics (Fluids in Motion)" (1958). Robert Katz Publications. 143.
[3] Surface tension and the origin of the circular hydraulic jump in a thin liquid filmAlexis Duchesne, Anders Andersen, Tomas Bohr
[4] S.K. Bhunia and J.H. Lienhard V, "Surface Disturbance Evolution and the Splattering of Turbulent Liquid Jets," J. Fluids Engineering, Vol.116, No.4, 1994, pp.721-727. (PDF)
[5] A Miniaturized Circular Hydraulic Jump for Remote On-Line Fluid Mechanics Instruction

COOKING OIL BIOFILTER BASED ON TABOA FIBER (THYPA DOMINGENSIS)

Stênio Cândido Bezerra dos Santos Filho[1], Júlia Graziela Rocha do Nascimento[2], Guilherme Alves França Gomes de Albuquerque[3],
Colégio Militar do Recife, Av. Visc. de São Leopoldo, 198 - Cidade Universitária, Recife- Brazil, comsoc@cmr.eb.mil.br
Universidade Federal de Pernambuco, Av. Prof. Moraes Rego, 1235 - Cidade Universitária, Recife - Brazil, secci@ufpe.br

ARTICLE INFO

Gold medalist in BUCA IMSEF 2022

Awarded by Ariaian Young Innovative

Minds Institute , AYIMI

http://www.ayimi.org ,info@ayimi.org

ABSTRACT

In Brazil, oil consumption is about three billion liters per year and it is estimated that for every four liters consumed, one is discarded incorrectly, representing more than 700 million liters released into the environment without proper care annually. The present project seeks to create and evaluate the functionality of a biofilter made from Taboa (Typha domingensis) fiber for the adsorption of oils thrown in residential sinks. To achieve the objectives, comparative tests were performed with two hydrophobic materials: Paina and Taboa fibers, seeking to show the efficiency of Taboa compared to other material already researched as an oil adsorbent.

Keywords : *TBiofilter, Vegetable Oil, Taboa, Adsorption, Water Pollution*

1. Introduction

Water is one of the essential elements for life to exist, being present in 70% of the human body's composition and also covering 70% of planet Earth. However, the distribution of this resource is quite uneven among the different regions of the planet. In this sense, and considering only fresh water in liquid form, the most adequate and most used for human consumption, about 13% is found in Brazilian territory. Therefore, we are well served by this vital element (OECD, 2015; UN, 2021).

Despite all the amount of water in the country, it is not available to all due to geographical and economic factors, and even in places where water exists abundantly, it is not suitable for human consumption, which occurs more evidently in urban centers, as in the case of Recife, which despite having about 99 urban channels and five major river has a system of water rotation for its inhabitants. (GALINDO, 2009; SOUZA, et al, 2018).

According to the World Water Resources Development Report, 2021, conducted in cooperation, by different UN Agencies, water consumption on the planet has increased 6 times in the last century and continues to increase about 1% per year, resulting from population growth, economic development and changes in consumption patterns among different societies. At the same time that the demand for the resource increases, the quality of the water drastically increases the reality of water scarcity, which already affects more than 2 billion people around the world and Brazil is one of the countries that stand out in this regard. Still according to the UN (2021), it is estimated that water consumption will increase by 25% by 2030.

In addition to the physical or economic scarcity of water, the lack of this resource also occurs due to the increasing degradation of water sources and bodies of water, mainly as a result of human actions. Among the forms of water degradation, the discharge of different types of oils causes great concern, because they produce adverse effects on fauna, flora, and human life, and when it occurs on a large scale, it also affects the economy, tourism, and even daily activities. It is important to highlight that oil is one of the wastes that has a high power of contamination when thrown directly into river courses through disposal in the trash or in the drains of sinks. (BRASIL, 2010; SOUZA, et al, 2018; SILVA et al, 2021)

Given the above, this research seeks, from laboratory experiments, to evaluate the use of the taboa fiber (Typha domingensis), to create a mechanism for filtering oils dumped in household sinks.

In the history of evolution of human society, oils represent an extremely relevant resource and considering vegetable oils, their importance is not only for their use in gastronomy, but also for economic, political and biological reasons. From the Mesopotamian and Ancient Greek peoples to the present day, the use of oil plays a relevant role, since it has the most diverse applications, whether for heating, illumination, food, cosmetics production or even energy production (SANTOS, 2020).

Considering only the edible oils, according to data from the German consulting company, Oil World, the world per capita consumption of domestic oil is, on average, fifty milliliters per day. As far as Brazil is concerned, oil also plays an important role, since about three billion liters are consumed per year, according to the Brazilian Association of Vegetable Oil Industries (ABIOVE, 2022).

However, it is important to highlight that oils are highly polluting substances and with great capacity to degrade ecosystems, especially aquatic ones, because due to its chemical composition, oil is immiscible with water, i.e., they do not mix, and oil is lighter (less dense) than water and when they mix, oil stays on top of water.

On a scale of environmental impact, edible vegetable oil is less polluting than oil of fossil origin such as petroleum, however, the contamination of water by edible oil causes damage to the functioning of the 9 water and sewage treatment plants and makes waste treatment more expensive by up to 45% and the part that remains in rivers may cause soil sealing, this still contributes to the occurrence of floods. (SOUZA,2018).

Despite causing great negative impact on one of the vital elements for life, the disposal of oils in household sinks is still a silent problem that deserves more attention, debate and environmental awareness, with a view to finding solutions that add up to the protection of water resources

2. Aim and Problem Question

Lately, news about oil spills in aquatic environments has become more and more frequent and society as a whole has turned its attention to this environmental problem. In this

sense, it is important to include in this debate the problem of edible oils being thrown into the sewage system through domestic sinks.

Research data from SABESP 2022 indicate that only 1 liter of oil can contaminate 25 thousand liters of water. The oil substances are not dissolved in water and, if discharged into river courses, they cause oxygen depletion and the death of aquatic species. In contact with the soil, the oil also causes contamination, not to mention the enormous damage caused by the accumulation of oil residues in the pipes of domestic sinks, which can cause serious problems for the maintenance of the networks and higher costs to make repairs and repairs (SABESP, 2022). (Fig.1).

Fig. 1: Release of edible oils in sinks Source: Alves & Araújo (2016)

In this sense, among the residues discharged into the collecting networks, lipids occupy the place of greatest pollutant of the sewage among the other materials, with about 60% of the contamination. In this context, the oil that has as final destination streams, rivers, and seas, promotes processes of environmental imbalance such as the eutrophication of water bodies and aquatic contamination in coastal areas. The discharge of oil into water bodies can also impede gas exchange and the passage of sunlight, impair breathing and photosynthesis of life submerged in a river, leading to the reduction of aquatic life or even the extinction of some of them.

In addition, oil pollution makes water treatment up to 45% more expensive, and aggravates the greenhouse effect, since the contact of water polluted by oil when flowing into the sea generates a chemical reaction that releases methane gas, a much more aggressive component than carbon dioxide. This is extremely serious when we analyze that the Brazilian federal government spends more than 600 million dollars on water treatment (ARCOVERDE,2022).

Despite being a long-debated topic, the solutions presented are still palliative or not very efficient, as in the case of storing oil in containers for later disposal and recycling, a solution that is still not very common among most Brazilians (SABESP,2022).

Data from the report of the Brazilian Association of Vegetable Oil Industries (ABIOVE) indicate that only 10% of the oil consumed in Brazil is recycled. One of the possible reasons for the low household oil recycling numbers may be the need to always have a pet bottle handy and also that the consumer has to store and deliver the product later to collection environments. Thus, the disposal process for possible reuse does not correspond to the population's perspectives and ends up being an inefficient measure since it is neglected by most users of cooking oils (ABIOVE, 2022) .

Also, according to Abiove, the consumption of edible vegetable oils in Brazil is around three billion liters per year and for every four liters consumed, one is discarded incorrectly, which represents more than 700 million liters per year thrown into the environment without proper care and control (ABIOVE, 2022).

Regarding legislation, the National Policy on Water Resources (PNRS) defines cooking oil as solid waste. For, although the oil has a liquid consistency, in contact with water it solidifies. Also, because it is a discarded waste from human activities, which is contained in a container and because it is not feasible to dispose of it in the public sewage system or in water bodies (BRASIL, 2010) (Fig.2).

Fig. 2: Flow of incorrectly discarded oil Source: Siqueira & Plese (2021)

Aiming to solve the environmental problem exposed, it is believed that the creation of a portable mechanism, capable of retaining the oil dumped in household sinks may present itself as an efficient solution. Thus, the hypothesis of this project is that the taboa fiber may be the ideal product for production in a biofilter for adsorption of cooking oil.

The objectives of the work are to produce and evaluate the use of a biofilter based on Typha domingensis (Typha domingensis) fiber for the adsorption of cooking oil thrown into household sinks and, consequently, into rivers. Analyze the viability of the taboa as oleophilic material for adsorption of lipids; Create prototypes of biofilter based on the taboa fiber with low-cost material for absorption of edible oil. Comparing the efficiency of the taboa fiber as an adsorbent of edible oil in comparison with the Paina fiber (Ceiba Pentandra), are part of the research needs.

As a theoretical basis, we took as reference the work developed by Oliveira (2010), in which the author conducted experiments to evaluate the solvent capacity of plant fibers from different species, including the aquatic macrophyte taboa (Typha domingensis).

The cattail (Typha domingensis) is a macrophyte that occurs naturally in freshwater environments. It is a perennial, herbaceous plant native to South America, with a cylindrical stem, averaging 1.5 m in height. It is quite abundant and produces about 7,000 kg of fruits (rhizomes) per hectare. Despite reproducing in a degraded environment, its rhizomes are edible, possessing protein value equal to that of corn and carbohydrates equal to that of potatoes (MOGROVEJO, 2019) (Fig. 3).

Fig. 3: Taboa plants in a construction site cavity Source: Authors (2022).

Aquatic macrophytes plants, such as Taboa, are widely used for the purpose of reducing contaminant loads and improving the quality of wastewater, because they act as biofilters in the removal of pathogenic microorganisms from the water and in the treatment of water with high load of pollutants, presenting high absorption of organic matter. The aquatic macrophytes also play the role of primary producers, providing habitat and refuge for several species of animals and also act as a substrate for algae, supporting the chain of detritus and herbivory and serving as a nutrient storage compartment (KREBS et al, 2021).

In addition to acting in water purification, Taboa is also considered an excellent adsorbent of oils, mainly from its fruit. This functionality of the plant is due to its high degree of hydrophobicity, buoyancy and high content of lipids 2.41% in its structure, providing significant surface adsorption of different types of oils, considering that the fruit has few empty spaces in its structure (OLIVEIRA, 2010).

The taboa fiber contains about 33.95% cellulose, 33.24% hemicelluloses, between 1.62% lignin, 2.06% ash and a moisture content of 9.33%. Taboa fruit has about 46.6% carbon, 5.96% hydrogen and 1.11% nitrogen and these properties contribute to lipid adsorption. (KHAN et al, 2004; Oliveira, 2010; MOGROVEJO,2019). Research attests the efficiency of the taboa fiber as an adsorbent of oils, however, tests and application of this fiber as a biofilter for sorption of edible oil were not found in the literature, which increased the interest in developing the present work. Thus, and considering that the main alternatives used to reduce the impacts resulting from the degradation of aquatic environments by edible oil spills still do not present significant results, it is expected, with this research, to contribute to the debate about the importance of developing alternative and low-cost methods that can reduce the damage caused by the release of oils in river courses using the taboa fiber.

3. Materials and Methods

Three stages were defined for the execution of the project, specified below.

Stage I: Data survey and creation of biofilter models.

The data was researched on sites of agencies and entities that work in the search for solutions to the problem of degradation of water sources and its causes, especially from the release of oils.

Based on the theoretical research, an oil sorption biofilter model was developed, considering the dimensions of different types of domestic sink drains used in Brazil. Two types of drains were chosen to create the biofilter prototype.

Stage II: Selection of the oleophilic filter material.

The choice of the Taboa tree fiber was based on the results obtained by other researches regarding biodiesel sorption and also because it is abundant and easy to find in nature. In order to carry out comparative tests, besides the Taboa tree, it was also selected Paina fiber (Ceiba Pentandra), a material already tested for the sorption of different types of oil, including vegetable oil (Fig. 4).

Fig. 4: Test material. Source: Authors (2022)

Stage III: Prototyping and testing with the use of taboa and kapok fibers and tulle fabric.

The biofilters were tested in reused coffee capsule containers, pet bottles, and disused sink drains.

For each filter half of a Taboa fruit was used. The fruit was loosened, crushed, and the fiber was placed inside each prototype. In the filter with the kapok fiber, half a fruit fiber was used. The fibers received lemon drops, were placed for drying and in perforated containers simulating sink drains (Fig. 5).

Fig. 5: Containers used to support the biofilter. Source: Authors (2022)

To analyze the functionality of the biofilters, five types of tests were performed, as described below (Table 1).

Table 1: test objectives performed, Recife. Source: Authors (2022)

	experiments performed in the laboratory
test 1	analyze water circulation
test 2	comparison of efficiency between diferent fibers
test 3	comparison of efficiency between different layers
test 4	comparison with the use of lemon additive
test 5	evaluation of biofilter reuse

In experiment 1, the circulation of water through Taboa and Paina biofilters prototypes was verified (Fig. 6).

Fig. 6: Prototypes of the biofilter. Source: Authors (2022)

In experiment 2, preliminary tests showed the adsorption of oil - pouring 200 ml of water and 50 ml of oil over each biofilter, the one with the Paina and the one with the Taboa fibers (Fig. 6), simulating the discharge of oil into sinks.

In experiment 3 the biofilter with a double layer of Taboa, without inserting lemon juice, was tested, seeking to verify the real capacity of oil adsorption by Taboa, the substance chosen for the biofilter.

In experiment 4, tests were performed at the Federal University of Pernambuco to compare the Taboa biofilters with and without the use of lemon (Fig. 7).

Fig. 7: Comparative test between double taboa filters with and without lemon at UFPE, Recife. Source: Authors (2022)

In experiment 5 the reuse of the Taboa biofilter was evaluated, after the oil adsorbed by the fiber was removed and the material was dried (Fig. 8).

Fig. 8: Water and oil solution after filtration. Source: the authors, (2022)

4. Results and Discussion

The tests indicate that the use of two layers of taboa fiber, forming a double filter, was more effective than the use of a single layer, being also more efficient than the biofilter of kapok fiber. The results obtained matched the results achieved by Oliveira (2010), when using the taboa fiber to absorb diesel oil. It is worth noting that the experimentation process cost only the value of one kilogram of lemon and 1m² of tulle to produce the biofilter prototypes.

After the experiments it was observed that the double Taboa fiber filter adsorbed about 49 ml of the 50ml poured and the water flowed without difficulty. Thus, the biofilter showed an average efficiency of 99% absorption, confirming the oleophilic property and hydrophobicity of Taboa, while the millet biofilter obtained an oil adsorption of about 60%. The part of oil (10 ml) that managed to pass through the Taboa filter presented a different coloration and the water had a clearer appearance (Table 2).

Table 2: corroborative results performed at UFPE, Recife.Source: Authors (2022)

Tests	Liquid Volume (ml)	Oil Retention Volume (ml)	Percentual Retention
1: biofilter with lemon	Oil(50 ml) Water(200 m	45 ml	80% of retention
2: biofilter without lemon	Oil(50 ml) Water(200 m	49 ml	98% of retention

These results indicate that the double biofilter made of woven wattle without the use of lemon has a higher efficiency than the others. It is important to emphasize that tests were also performed with the taboa fiber after the first use, attesting to the possibility of reusing the material, after cleaning and removing the absorbed oil.

The corroborating results attest to the effectiveness of the biofilter produced, being a viable and sustainable solution to the serious problems arising from the discharge of oil into river courses from households. After being used in the biofilters, the fibers of the Taboa and Kapok were stored in a container for later removal of the adsorbed oil. The plant material will be sent to Sempre Viva, a non-governmental organization that performs the separation of oil for soap production and the introduction of plant compounds in a biodigester system in order to synthesize fertilizer and biogas.

5. Conclusion

In view of the tests performed and the corroborating results achieved, it can be concluded that the taboa is a viable alternative as a material for making the oil filter for adsorption of household oils. For being an ecologically sustainable material, of low cost and easy to obtain, the taboa has its viability confirmed. So far, the experimentation has shown results within the authors' expectations and, as a further step, it is planned to introduce the use of the biofilter in 10 homes in order to monitor the performance of the biofilter in a real situation.

It is believed that an accessible, practical and innovative solution to the issue of domestic oil disposal is possible with the use of the Taboa biofilter. Thus, it is also expected that the research can contribute to the development of a sustainable alternative of easy development and application and low cost, aiming to considerably reduce serious socio-environmental problems such as the improper disposal of oil into the sewage system.

Finally, it is noteworthy that this research is innovative, considering that no literature has been found about the possible production of a biofilter made of Taboa bean. It is hoped that the product created will contribute to reduce the damage caused by the discharge of oil into rivers and contribute to a healthier environment for all, in close accordance with the Sustainable Development Goals proposed by the UN.

References

[1] Abdel-Ghani, N.T., Hegazy, A.K. & El-Chaghaby, G.A. Typha domingensis leaf powder for decontamination of aluminium, iron, zinc and lead: Biosorption kinetics an equilibrium modeling. Int. J. Environ. Sci. Technol. 6, 243– 248 (2009). https://doi.org/10.1007/BF03327628; ASSISOdilio Benedito Garrido de; SILVA, Wilson Tadeu Lopes da;

[2] MATTOSO, Luiz Henrique Capparelli; Rede de Nanotecnologia Aplicada ao Agronegócio Anais do V Workshop 2009, ISSN 2175-8395. Empresa Brasileira de Pesquisa Agropecuária, Embrapa Instrumentação Agropecuária, Ministério da Agricultura, Pecuária e Abastecimento, São Carlos, SP-2009. Disponível em: https://docplayer.com.br/116816713-Rede-de[1]nanotecnologia-aplicada-ao-agronegócio-anais-do-v[1]workshop-2009.html;

[3] ECÓLEO – Associação Brasileira para Sensibilização, Coleta, Reaproveitamento e Reciclagem de Resíduos de óleo Comestível. Ecóleo, 2018. Reciclagem. Disponível em https://ecoleo.org.br/projetos/6766-2/, acessado em: 22 de julho de 2022 ;

[4] HEGAZY, A.K., Abdel-Ghani, N.T. & El-Chaghaby, G.A. Phytoremediation of industrial wastewater potentiality by Typha domingensis . Int. J. Environ. Sci. Technol. 8, 639–648 (2011). https://doi.org/10.1007/BF03326249.;

[5] KHAN, E.; VIROJNAGUD, W.; RATPUKDI, T. Use of biomass sorbents for oil removal from gas station runoff. Journal Chemosphere, v. 57, p. 681-689, 2004. ;

[6] MOGROVEJO, Wendy Alejandra Montenegro. Uso de taboa para o tratamento de águas residuárias e produção de biogás(Dissertação). Faculdade de Ciências Agronômicas da Unesp, Botucatu, 2019;

[7] OECD (2015), Governança dos Recursos Hídricos no Brasil, OECD Publishing, Paris . http://dx.doi.org/10.1787/9789264238169-pt. ISBN 22 978-92-64-23816-9(PDF).

[8] OLIVEIRA, Adriana Ferla de. Avaliação de desempenho de fibras lignocelulósicas na sorção de óleos diesel e biodiesel. 2010. xviii, 98 f. Tese (doutorado) - Universidade Estadual Paulista, Faculdade de Ciências

[9] OLIVEIRA, Leonardo Mendonça Tenório de Magalhães. Caracterização e avaliação das fibras de paina (Ceiba pentandra (L.) Garten do nordeste brasileiro na sorção de óleo diesel /Leonardo Mendonça Tenório de Magalhães Oliveira 2020. Disponível em: https://www.repositorio.ufal.br/handle/riufal/6934 OLIVEIRA, Leonardo M.T.M.;

[10] OLIVEIRA, Laís F.A.M. et al. Ultrafast diesel oil spill removal by fibers from silk[1]cotton tree: Characterization and sorption potential evaluation; Elsevier Journal of Cleaner Production, Volume 263, 1 August 2020, 121448. Universidade Federal de Alagoas- Maceió, AL. Disponível em: https://www.sciencedirect.com/science/article /abs/pii/S095 9 652620314955.

[11] ONU - Relatório mundial das Nações Unidas sobre desenvolvimento dos recursos hídricos 2021: o valor da água; fatos e dados. Programa Mundial da UNESCO para Avaliação dos Recursos Hídricos. Escritório do Programa de Avaliação Global da Água. Divisão de Ciências da Água, UNESCO, Colombella, Perúgia, Itália,2021.

[12] SILVA, Victor Gustavo Diniz,et al. Avaliação do uso de fibra vegetal oleofílica na coleta de óleo derramado em ambientes aquáticos. Anais Feira Brasileira de Ciências e Engenharia (FEBRACE), USP,São Paulo, 2021.

[13] SIQUEIRA, Reinaldo Maia; PLESE, Luís Pedro de. Resíduo de óleo de cozinha: estudo de caso no bairro Xavier Maia - Rio Branco/AC.Brazilian Journal of Development, Curitiba, v.7, n.5, p. 47577-47594 may. 2021

[14] SOUZA, Nataly Maria de Oliveira;et al. Impactos ambientais causados pelo descarte inadequado do óleo de cozinha e as suas formas de reuso. VI Congresso Internacional das Licenciaturas- COINTER- PDVL, 2018. Anais.

[15] WANG, Jintao; WANG, Hongfei; Eco-friendly construction of oil collector with superhydrophobic coating for efficient oil layer sorption and oil-in-water emulsion separation; Elsevier- Surface and Coatings Technology, Volume 350, 25 September 2018, Pages 234-244. North Minzu University, China- 2018. Disponível em: https://www.sciencedirect.com/science /article/abs/pii/ S0257897218307138

SPINNING OR SLIDING OF A WASHER ON A VERTICAL ROD

Ramin Abdollahzadeh, Mofid 1 high school, Tehran, Iran, raminabdollahzadeh8@gmail.com

ARTICLE INFO

Participated in PYPT, IYPT 2022

Advisors: Alireza Noroozshad, Hirad Davari

Accepted in country selection by Ariaian Young Innovative Minds Institute , AYIMI

http://www.ayimi.org ,info@ayimi.org

ABSTRACT

The motion of the washer on a vertical steel rod is investigated which may start spinning instead of simply sliding down. Terminal velocity of this movement and other affective parameters are considered by different experiments. It is possible to observe the washer will start to rotate on the rod by an initial velocity and rotate till it reaches a maximum angle and a steady state for the washer's rotation and finally reaching to the point that we can perceive a free fall motion for the washer's movements .

Keywords : *Terminal Velocity, Washer, Kinetic Energy*

1. Introduction

The problem states that a washer on a vertical steel rod may start spinning instead of simply sliding down. To study the motion of the washer and what determines the terminal velocity with the most parameters that would affect on it, several experiments are designed .

To find the optimum conditions different rods and washers are studied.

2. Theories and Methods

Starting with initial observation and introduction of the phenomenon, the main purpose of the statement is to investigate the terminal velocity and the parameters that would affect the terminal velocity of the washer, it is possible to observe that the washer will start to rotate on the rod by an initial velocity and it will rotate till it reaches a maximum angle and a steady state for the washer's rotation and finally reaching to the point that we can perceive a free fall motion for the washer's movements.

To start the basic theory and to have a better intuitive view of the phenomenon, amplitude of the sound that is possible to hear by the washer's movements on the rod is recorded (Fig. 1).

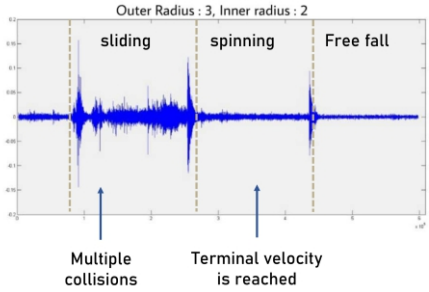

Fig. 1: Recorded sound of washer movement on the rod

The basic transition between the motion of the washer will be sliding motion which involves acceleration and tilting of the washer around the rod. It is expected to be a free fall motion but will turn into a spinning motion which is possible to observe different types of angular velocity in different conditions.

Terminal velocity of the system leads us to a maximum tilt angle . By tracker the change of the angle per time and the maximum tilt angle are measured. Having a schematic observation of the contact points, 3D printed washer designed to see that there are two contact points.

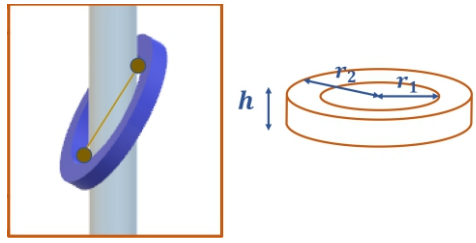

Fig. 2: Washer's dimensions and its contact points on the rod

The main motion of the washer will be rotating around the rod that we can divide this motion to two different motions one in z direction and the other one in "x,y" which makes the phenomenon more clear.

A theory based on energy determines the velocity of the system but this theory will be in the steady state condition that the angular velocity of the system is stable . Each term of the equation is investigated and we will start with the air resistance which by estimation is negligible.

Now to divide each kinetic energy that affects on the washer's movements, there are two kinetic energies. One of them is based on the angular velocity in different directions z and x, y. The other kinetic energy is based on terminal velocity of the washer, but because the rotational energy , this formula represents the equation for inertia in z and x, y components (Eqs.1-5).

$$k_1 + k_2 + \frac{1}{2}mv_z^2 - mg(v_z t) + \mu N(r\omega_{xy} t) + \cancel{W_{air}} = \text{cte} \quad (1)$$

$$E = k_1 + k_2 + \frac{1}{2}mv_z^2 - mg(v_z t) + \mu N(r\omega_{xy} t) \quad (2)$$

$$E = \frac{1}{2}I_{xy}\omega_{xy}^2 + \frac{1}{2}I_z\omega_z^2 + \frac{1}{2}mv_z^2 - mg(v_z t) + \mu N(r\omega_{xy} t) \quad (3)$$

$$I_{xy} = \frac{1}{12}m(3(r_2^2 - r_1^2) + h^2) \quad (4)$$

$$I_z = \frac{1}{2}m(r_2^2 - r_1^2) \quad (5)$$

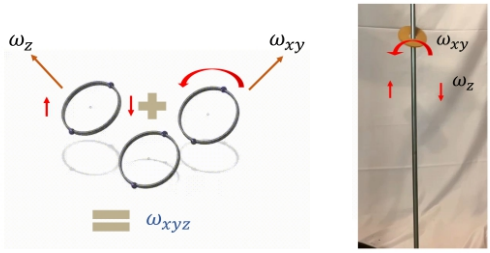

Fig. 3: The angular velocity of the washer in different directions

The equation for energy of the system involves the terminal velocity in z component due to the change of velocity based on change of washer's, and we obtain the terminal velocity in z component by this equation. By observing the motion in steady state from the experiment we can get a better intuitive view of the condition that the energy stays constant and why the equation from the qualitative theory is based on the fact that the motion is stable in the steady state (Eqs. 6-8).

$$v_z = \frac{D_{rod}}{2\pi}.(\omega_{xy}+\omega_z) \quad (6)$$

$$D_{rod} = 1cm$$

$$\frac{D_{rod}}{2\pi}.(\omega_{xyz}+\omega_{xyz}) - \mu N r \omega_{xy} = 0 \quad (7)$$

$$E = k_1 + k_2 + \frac{1}{2}mv_z^2 - mg(v_z t) + \underbrace{\mu N}_{mg\cos\alpha}\underbrace{(r\omega_{xy}t)}_{\substack{\text{rotation time in} \\ \alpha_{max}\ \text{condition}}} \quad (8)$$

0.8

3. Experiment

In our experimental setup 64 different sizes for washers are used.

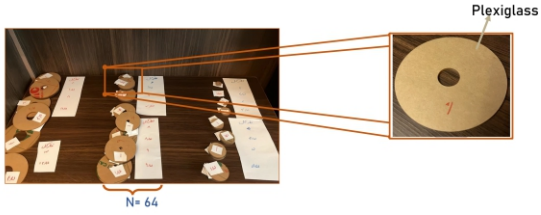

Fig. 4: Plexiglass washers in 3 mm thickness

The energy and terminal velocity in steady state for different washers and the time range of movement are calculated according to the theory for 25 different plexiglass washers that the longest time for the washer rotation belongs to washer number 9 (Diameter 6 cm and hole diameter 3 cm) (Figs. 5-7).

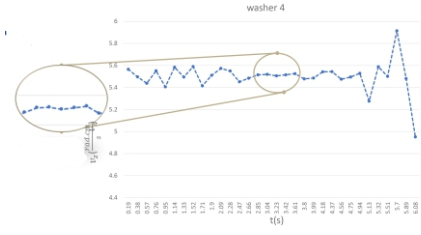

(a)

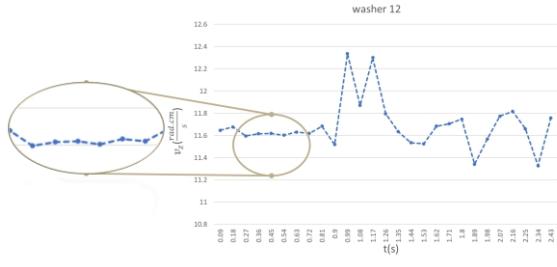

(b)

Fig. 5: Terminal velocity of washers in two samples a) washer No 4 , b) washer No12

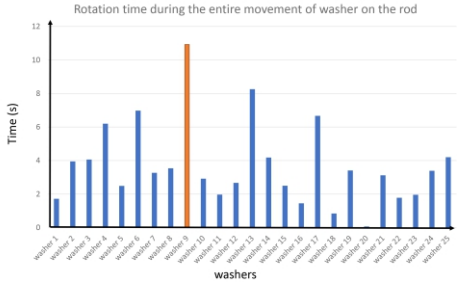

Fig. 6: Rotation time of different washers

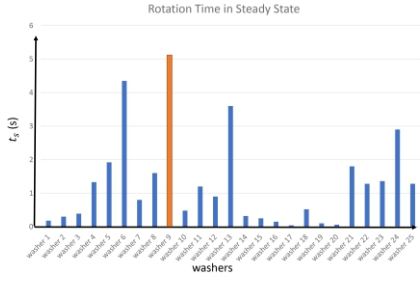

Fig. 7: Rotation time of different washers in steady state

The same experiment goes for the velocity of each washer in z component, and by the result of the experiment, the most displacement in z direction belongs to washer No17, but as the main investigation in steady state, as much as the terminal velocity in z axis decreases for instance the washer No3, the time that the washer stays in steady state increases (Fig. 8).

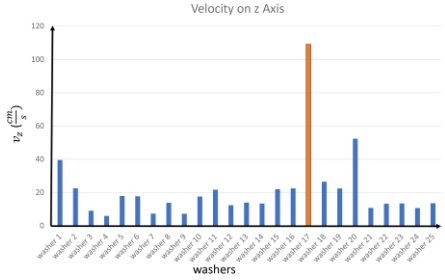

Fig. 8: Velocity of different washers on Axis Z

4. Conclusions

In this research we found several parameters regarding different washers movement on the rod including time range in steady state, which clarifies the time of start of the

state till the end of it.

To start the basic of the theory and to have a better intuitive view of the phenomenon, we used amplitude of the sound that is possible to hear by the washer's movements on the rod and a basic transition between the motion of the washer will be sliding motion which involves acceleration, tilting of the washer around the rod and it will turn into a spinning motion and after that we expect a free fall motion and it is possible to observe different types of angular velocity in different conditions. Tracker and 3D printed washer is used to measure the change of the angle per time and the maximum tilt angle. To determine the velocity of the system theory based on energy is used . But this theory is in the steady state condition that the angular velocity of the system is stable for different washers. The comparison between theory and the experiment shows a good agreement.

References

[1] https://byjus.com/jee/perpendicular-axis-theorem/

[2] https://courses.lumenlearning.comsuny-osuniversityphysics/chapter/10-4-moment-of-inertia-and-rotational-kinetic-energy/

HOW TO MAKE A CANDLE POWERED TURBINE

Seyed Zahra Hosseini Alghadir high school, Kish Island, Iran, thetomycat@gmail.com

ARTICLE INFO

Participated in PYPT, IYPT 2022

Advisors: Alreza Noroozshad, Rojan Abdollahzadeh Mirali

Accepted in country selection by Ariaian Young

Innovative Minds Institute , AYIMI

http://www.ayimi.org ,info@ayimi.org

ABSTRACT

As demonstrated in this research, to make a turbine by a candle under a spiral it starts to rotate above the needle that is attached to the tip of the rod so, we can say the spiral above the candle rotates by the air flow that comes from the heat that is given to it by the candle. But to investigate this phenomenon , different experiments have been done and the most important parameters related to the characteristic of spiral,candle and heat transfer are studied.

Keywords : *Candle, Turbine, heat Transfer, Spiral*

1. Introduction

The problem states that a paper spiral suspended above a candle starts to rotate optimize the setup for maximum torque (Fig.1).

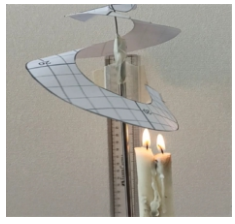

Fig.1: Paper spiral suspended above a candle

The candle under the spiral lit up, spiral starts to rotate above the needle that is attached to the tip of the rod so, we can say the spiral above the candle rotates by the air flow that comes from the heat that is given to it by the candle. The candle heats the surrounding air heated air causes the air particles to go farther apart. Thereby, making the air less dense and less dense air always rise above the dense air.

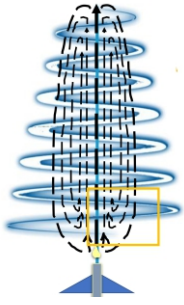

Fig.2: Heat transfer around the spiral

2. Materials and Methods

To analyze this setup in a theoretical way initially we're going to start with the spiral itself that is divided into 3 parts we can name:

1. Number of the spiral cycles
2. Radius of the spiral circle
3. The paper width

As the second part of the theory analyzing, we will discuss about the convection mechanism and the effects on the phenomenon, then the candle that is divided into three parts:

1. candle wax combustion
2. candle flame
3. the causes effect from the distance between candle and spiral

Moving to the division between our theories we can distribute them to two different viewpoints which are the macroscopic view and the microscopic view. First we start with the microscopic view to discuss the partial forces applied to the spiral and the transition between energies.

The heat conduction makes the burning fuel releases CO_2 and Water and the steam as well as the heat radiation causes the air molecules to run parallel to the spiral (Fig. 3).

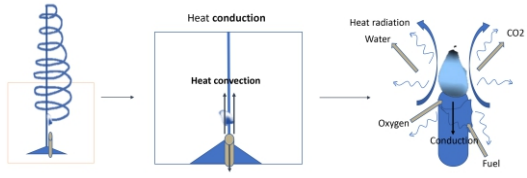

Fig.3: Burning fuel and heat radiation

Wax combustion makes turning thermal energy into kinetic energy of the air particles.

$$C25H52 + 38\,O2 \rightarrow 25\,CO2 + 26\,H2O + Heat$$

So to divide each applied force to the system the definition of the drag force is needed. The applied force by the particle is an action force and a reaction force is from the opposite direction. The air particles begin to rotate in the direction of motion (Fig. 4).

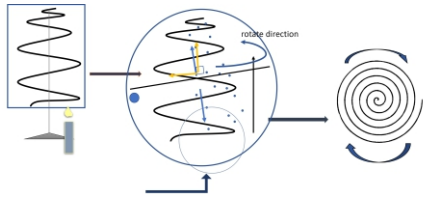

Fig.4: Rotation of spiral

To name each force that is applied to the strip part of the spiral, we can see as the laminar flow runs throw the strip it goes up with a turbulent form, and the force from air flow is divided into one in the direction of motion and one perpendicular to the strip which makes a total force which applies into the torque according to the changes of spiral radius (Eqs. 1-3) .

$$\tau = Fr\sin\theta \tag{1}$$

$$\Delta\tau = r\Delta F\sin\theta \tag{2}$$

$$\tau = \sum \Delta\tau = \sum r\Delta F\sin\theta \tag{3}$$

Fig. 5: Applied forces on spiral

Also there is a maximum torque by air transfer and friction which works on the opposite direction of motion (Eqs.4-6).

$$\tau = Fr \longrightarrow \tau = I\alpha \tag{4}$$

$F \sim v$

$$\tau' = Fr \sim r^2\omega \tag{5}$$

$$\tau' = \tau \tag{6}$$

The macroscopic view which is the definition of air transfer and starts with convection is the circular motion that happens when warmer part of fluid rises while the cooler part of fluid drops down.

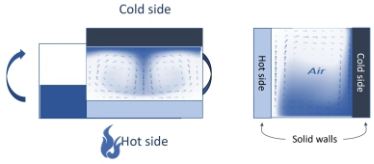

Fig. 6: Microscopic view of convection

As the warm air rises upward the paper begins to spin, the process keeps working because the cooler surrounding air keeps coming towards the candle and warms up. But of course, there is a difference between two parts of the spiral from down to upside part and that is where the area of air flow starts to increase and the velocity of the movements decreases (Eq. 7) (Fig.7).

$$A_1V_1 = A_2V_2 \tag{8}$$

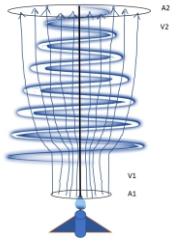

Fig. 7: Modeling of air flow around the spiral

Having an intuitive view of the Continuity equation a simulation of velocity for each air particle is done. If we have an imaginary closed area around the spiral to avoid other effective parameters such as wasted air flow that gets out of the spiral area, as the solution for air particles velocity , we can observe the movements of the particles are not the same in every part of the spiral and the velocity streamline divided these speeds into different colors is possible to see in the model itself (Fig. 8).

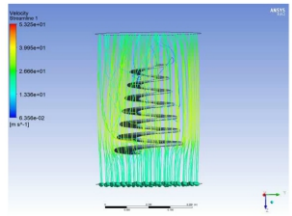

Fig. 8: Simulation of velocity for each air particle

3. Experiments

The microscopic view of the theory in our experiment proves the reason for the spiral to rotate regularly with almost constant speed which helps to find a version of transition between airflow.

The schlieren photography shows there are two different types of air flow, laminar and turbulent . As the experiment shows as the spiral appears the laminar flow transforms into turbulent flow including the air currents or we can say turbulent flow moves around the spiral (Fig. 9).

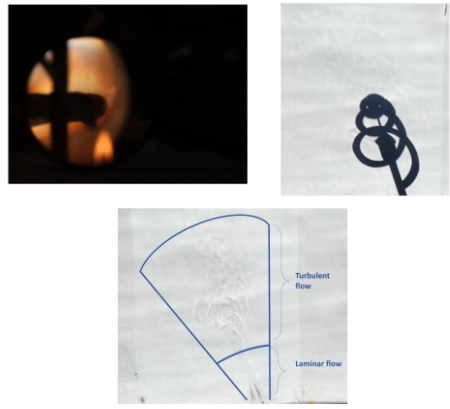

Fig. 9: The schlieren photography

In our Experiment the spiral is divided into a 4 different number of cycles and 4 different densities for each number of cycles with a needle is attached to the rod to keep the friction as less as possible .The candle is in three different distances from the rod to see the result .Further, we used tracker to measure the radiation of the spiral and it is analyzed by the Fourier transformation (Fig. 10) .

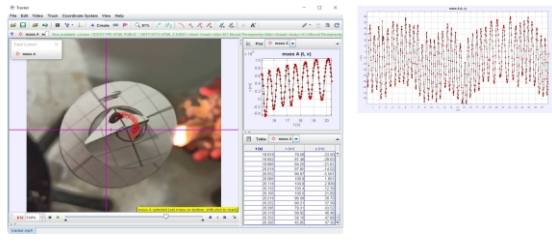

Fig. 10: Tracker to analyze data

For the next part of the experiment, density and angular velocity of the strip from 1 cm to 2.5 cm are investigated. In each experiment by the change of number of rounds, when the density\width of the strip for paper spiral increases, there is a decreasing trend in the graphs which occurs for each number of rounds from 4 to 7 (Fig. 11).

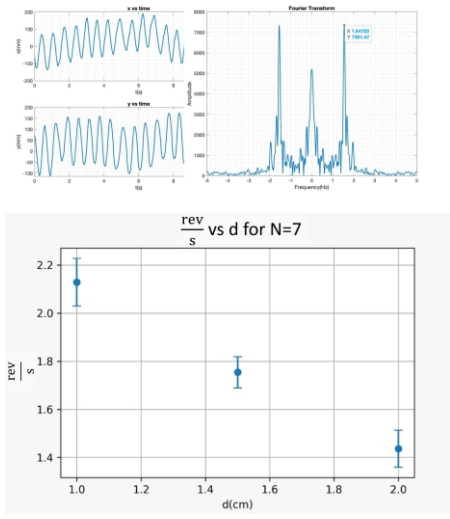

Fig. 11: Changing density and angular velocity

4. Results

It can be reported that by increasing the density of the strip, rotating per second for that specific spiral is decreasing. The same thing happens for the number of rounds, five, and the change of the density in the same way and there is almost an decreasing trend by increasing the density. Best change and almost close to the theory is given in the diagram for number of rounds six with the least error of the experiment which is possible to observe a more logical decrease of angular velocity of the system, the same experiment goes for number of rounds 7 but to mention that density, 2.5 cm couldn't be investigated for this spiral because of the weight of the strip which I couldn't measure. Each experiment for each density of the spirals is done four times to make sure that the variation of angular velocity for the same spiral has a little error.

As the result of the experiment, the color-coded version is used to show 9 different number of rounds by the different density and divergent number of cycles. The velocity will decrease by increasing the number of rounds or density for each number of rounds.

A color-coded approach from the experiment represents the state of the rotational speed for each spiral. The green stands for the best and the fastest ones as it is possible to see in the intuitive view of the experiment, the light green section is consider as the well rotation and between the time range of 1.5 to 1.7 for each rotation in this phenomenon, and the yellow section is representation of the 1.7 to 2.5 seconds for each rotation of the spiral (Fig.12).

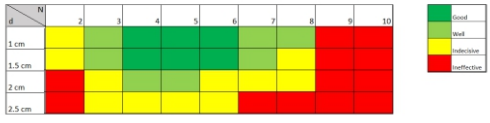

Fig. 12: Color coded approach

An optimization for the best setup in this experiment I reached to two best setups that the speed of the rotation had the best result, and it is possible to observe by the experiment in the video of each spiral for maximum torque. (Fig 13).

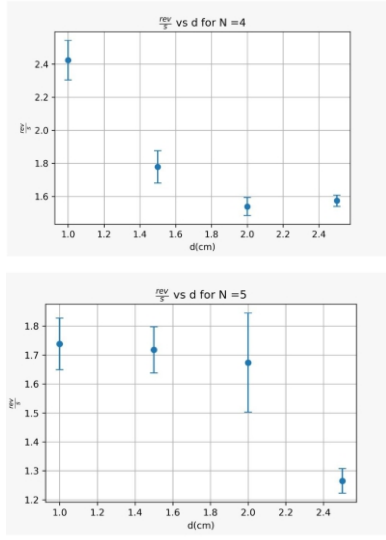

Fig. 13: The best spiral for maximum torque

5. Conclusions

This research by the theory in energy transition and the division between forces applied to the system and obtaining each force. Total torque equation and the factors to have a maximum torque and the study of airflow that causes the force were studied. For the experiment to measure the maximum torque four number of rounds with different densities of the strip for each spiral have been used. The result of the experiment by a color-coded version for the diagrams and optimized the setup for maximum torque between the best experiment and angular velocities have been presented that was gotten from the green code experiments.

References

[1] https://www.thoughtco.com/where-does-candle-wax-go-607886

[2] https://stemfellowship.org/iypt-references/problem13/ Cross, Rod. "Rotating Ring on a Vertical Rod." Physics Education 56, no. 2 (2021): 023003. https://doi.org/10.1088/1361-6552/abd992.